



**QUEEN'S
UNIVERSITY
BELFAST**

Climate and environment in southwest Sweden 15.5 – 11.3 cal. ka BP

Wohlfarth, B., LUOTO, TOMI. P., Muschitiello, FRANCESCO., VÄLIRANTA, M., BJÖRCK, S., Davies, S. M., ... SMITTENBERG, RIENK. H. (2018). Climate and environment in southwest Sweden 15.5 – 11.3 cal. ka BP. *Boreas*, 47(3), 687-710. <https://doi.org/10.1111/bor.12310>

Published in:
Boreas

Document Version:
Peer reviewed version

Queen's University Belfast - Research Portal:
[Link to publication record in Queen's University Belfast Research Portal](#)

Publisher rights
Copyright 2018 Wiley. This work is made available online in accordance with the publisher's policies. Please refer to any applicable terms of use of the publisher.

General rights
Copyright for the publications made accessible via the Queen's University Belfast Research Portal is retained by the author(s) and / or other copyright owners and it is a condition of accessing these publications that users recognise and abide by the legal requirements associated with these rights.

Take down policy
The Research Portal is Queen's institutional repository that provides access to Queen's research output. Every effort has been made to ensure that content in the Research Portal does not infringe any person's rights, or applicable UK laws. If you discover content in the Research Portal that you believe breaches copyright or violates any law, please contact openaccess@qub.ac.uk.

Climate and environment in southwest Sweden 15.5 – 11.3 cal. ka BP

BARBARA WOHLFARTH, TOMI P. LUOTO, FRANCESCO MUSCHITIELLO, MINNA VÄLIRANTA, SVANTE BJÖRCK, SIWAN M. DAVIES, MALIN KYLANDER, KARL LJUNG, PAULA J. REIMER AND RIENK H. SMITTENBERG

Wohlfarth, B., Luoto, T. P., Muschitiello, F., Väliiranta, M., Björck, S., Davies, S. M., Kylander, M., Ljung, K., Reimer, P. J. & Smittenberg, R. H.: Climate and environment in southwest Sweden 15.5 - 11.3 cal. ka BP. *Boreas*, Vol. 00, pp. 0-00.

Lake sedimentary records that allow documenting the distinct climatic and environmental shifts during the early part of the Last Termination are scarce for northern Europe. This multi-proxy study of the sediments of Atteköpsmosse, southwest Sweden, therefore fills an important gap and provides detailed information regarding past hydroclimatic conditions and local environmental responses to climatic shifts. Lake infilling started *c.* 15.5 cal. ka BP, but low aquatic productivity, cold summer lake water temperatures, unstable catchments and scarce herb and shrub vegetation prevailed until *c.* 14.7-14.5 cal. ka BP. Inflow of warmer air masses and higher July air temperatures favoured a rise in aquatic productivity and lake water summer temperatures, and the establishment of a diverse herb, shrub and dwarf shrub vegetation, which also included tree birch *c.* 14.5 cal. ka BP. Freshening of the moisture source region *c.* 13.7-13.6 cal. ka BP does not seem to have had a large impact on the ancient lake and its catchment, since lake aquatic productivity increased further and lake water summer temperatures and minimum mean July air temperatures remained around 12-14 °C. In contrast, further freshening of the moisture source region *c.* 13 cal. ka BP triggered a decrease in lake productivity, drier conditions and lower lake water summer temperatures. Macroscopic finds of tree *Betula* and *Pinus sylvestris* at 13-12.8 cal. ka BP demonstrate the presence of these trees in the lake's catchment. The transition into the Holocene (11.6-11.5 cal. ka BP) is marked by a change in chironomid assemblages and by a rise in lake water summer temperatures and aquatic productivity. These changes were followed by the re-establishment of a diverse aquatic and terrestrial vegetation, including tree birch and *Pinus sylvestris* at 11.4 cal. ka BP.

Barbara Wohlfarth (barbara.wohlfarth@geo.su.se), Svante Björck, Malin Kylander and Rienk H. Smittenberg, Department of Geological Sciences and Bolin Centre for Climate Research, Stockholm University, SE-10691 Stockholm, Sweden; Tomi P. Luoto, Division of Environmental Ecology, Department of Environmental Sciences, University of Helsinki, Niemenkatu 73, FIN-15140 Lahti, Finland; Francesco Muschitiello, Lamont-Doherty Earth Observatory of Columbia University, Division of Biology and Paleo Environment, 61 Route 9W – PO Box 1000, Palisades NY 10964-8000, USA; Minna Väliranta, Environmental Change Research Unit, Department of Environmental Sciences, P. O. Box 65, FIN-00014 University of Helsinki, Finland; Siwan S. M. Davies, Department of Geography, Swansea University, Singleton Park, Swansea SA2 8PP, Wales, UK; Karl Ljung and Svante Björck, Department of Geology, Sölvegatan 12, SE-22362 Lund, Sweden; Paula J. Reimer, Chrono Centre, School of Natural and Built Environment, Queen's University Belfast, BT7 1NN, United Kingdom.

More than four decades ago the question was raised whether parts of southernmost Sweden and in particular the higher parts of Kullen Peninsula and Hallandsåsen (Fig. 1A, B) had become ice-free very early during the last deglaciation (Berglund 1971, 1979; Berglund & Malmer 1971; Lagerlund 1977; Lagerlund *et al.* 1983; Sandgren 1983; Berglund & Mörner 1984). This hypothesis was supported by ages of >15 cal. ka BP and >14.5 cal. ka BP for the basal sediments in Atteköpsmosse on Hallandsåsen (Björck and Liedberg-Jönsson, unpublished; Håkansson 1984) and in Håkullsmosse and Björkerödsmosse on Kullen Peninsula (Berglund & Ralska-Jasiewiczowa 1986; Liedberg-Jönsson 1988) (Fig. 1A, B), respectively. Further ¹⁴C dates confirmed these early deglaciation ages (Sandgren *et al.* 1999) and suggested that some areas had become ice free already around 17 cal. ka BP (Sandgren & Snowball 2001). These age assignments and other regional observations were later incorporated in a reconstruction of Fennoscandian Ice Sheet growth and/or melt (Lundqvist & Wohlfarth 2001; Hughes *et al.* 2016; Stroeve *et al.* 2016). The recently published time slice maps of Hughes *et al.* (2016), which display maximum, mean and minimum positions of the ice sheet during the last deglaciation, thus indicate that parts of Kullen Peninsula and Hallandsåsen were ice free as early as 17 cal. ka BP (Fig. 1A).

With basal sediments dating back to >15 cal. ka BP, Atteköpsmosse (Fig. 1A-C) (Björck & Liedberg-Jönsson, unpublished; Håkansson 1984) offers the opportunity to expand the existing data sets from Kullen Peninsula (Berglund 1971; Berglund & Malmer 1971; Berglund & Mörner 1984; Berglund & Ralska-Jasiewiczowa 1986; Lemdahl 1988; Liedberg-Jönsson 1988; Hammarlund 1999) and to explore environmental responses to the large-scale hydro-climatic shifts that occurred at the end of the last glacial period. Our new multi-proxy study of Atteköpsmosse's lake sediments presented here combines lithostratigraphy, geochemistry, tephra, biomarkers and hydrogen isotopes, pollen stratigraphy,

plant macrofossils, chironomids and a high-resolution chronology. Together, these different proxies provide information on changes in lake status, vegetation, hydroclimatic conditions and summer temperatures between 15.5 and 11 cal. ka BP. Specifically, they allow shedding light on the local and regional climatic and environmental development during an early part of the last deglaciation, a time period that has not been investigated in such detail earlier.

Site description and fieldwork

Atteköpsmosse is located at 180-175 m a.s.l. on Hallandsåsen (56°23' N; 12°51' E) and close to the Swedish west coast (Fig. 1A-C). The area receives its precipitation mainly from the North Sea and the Nordic Seas (Gustafsson *et al.* 2010). Hallandsåsen is a NW-SE trending horst in south-western Sweden. Its bedrock is dominated by metamorphic basement rocks, which are intersected with pockets of magmatic dykes. Carbonate rocks (limestone, dolomite, marble) are found in low-lying areas to the north of the ridge. Sandy till originating from the last glaciation covers the bedrock; and wetlands and peatbogs are frequent in the western part of the horst system (Fig. 1C). Mean annual temperatures and mean annual precipitation (1961-1990) for the western part of Hallandsåsen were 7-8 °C and 800-900 mm a⁻¹, respectively (SMHI, 2017).

Atteköpsmosse is today a small wetland (Fig. 1C), which is surrounded by forested slopes, except for in the south-eastern part and covered by *Sphagnum*, sedges, birch and alder trees. Multiple sediment cores and three east-west transects performed in the years 1981 and 2000 allowed reconstructing the bottom topography and infilling of the wetland (Björck and Liedberg-Jönsson, unpublished; Ljung and Andersson, unpublished; Veres 2001). The long sediment core obtained in 1981 (C-1981) was analysed for loss-on-ignition and pollen (Björck and Liedberg-Jönsson, unpublished) and suggested basal ages of >15 cal. ka BP (Håkansson 1984). Investigations on cores from the central part of the basin (C-2000/C6) (Ljung and Andersson, unpublished) included loss-on-ignition, total organic carbon, magnetic susceptibility, grain size analyses and ¹⁴C dates and confirmed the earlier age of the basal sediments (Veres 2001).

In autumn 2011, we recovered a new series of sediment cores (C-2011) from the deepest part of the wetland using a Russian corer (7.5 and 5 cm diameter, 1 m length). To obtain sufficient material for all subsequent analyses, we opted for an overlap of 50 cm between successive core segments. The sediment cores were wrapped in plastic foil, placed in PVC tubes and transported to the Department of Geological Sciences, Stockholm University, where they were stored at 4 °C. Here we focus primarily on sediment core C-2011, but make use of the loss-on-ignition curve and the pollen stratigraphy that had been established on core C-1981 (Björck and Liedberg-Jönsson, unpublished).

Methods

The lithology of the ten individual core segments retrieved in autumn 2011 (C-2011) was described and overlapping cores were correlated with each other using specific marker horizons. This, combined with XRF scanning (see below), allowed creating a composite stratigraphy between 402 and 750 cm (Table S1) and formed the basis for further sub-sampling in autumn 2014. Prior to sub-sampling, we carefully cleaned the core surface by removing about 0.5-1 cm of the outermost sediment. Sub-samples were taken in contiguous 1 cm increments and split to accommodate for various subsequent analyses. One half of the samples was freeze-dried and used for analysis of loss-on-ignition (LOI), tephra, total organic carbon and carbon isotopes, chironomids, lipid biomarkers and hydrogen isotopes. The other half of the samples was utilized for plant macrofossil analysis and radiocarbon dating. Sediment core C-1981 had already earlier been described (Table S1), sub-sampled and analysed for LOI and pollen at 5 and 2-12 cm intervals, respectively and for ^{14}C dating (Björck and Liedberg-Jönsson, unpublished).

XRF scanning, loss-on-ignition (LOI) and tephra analysis

Scanning of the C-2011 cores was done at the Department of Geological Sciences, Stockholm University using an ITRAX XRF Core Scanner from Cox Analytical Systems (Gothenburg, Sweden). XRF analyses were made using a Mo tube set at 30 kV and 40 mA with a step size of 5 mm and a dwell time of 100 s. Based on analytical performance (counting statistics), reliable data were acquired for Si, S, K, Ca, Ti, Mn, Fe, Rb, Sr and Zr (Fig. S1). The single element data were transformed using a centred log-ratio (clr) function performed in CoDaPack (Comas-Cufí & Thió-Henestrosa 2011) following the work of Weltje & Tjallingii (2008) and Weltje *et al.* (2015). The selected elemental and ratio profiles shown here were smoothed using a 5-point running mean to capture the main shifts.

Samples for LOI measurements (at 550 °C) were dried over night at 105 °C, ground and then combusted at 550 °C for three hours. LOI was calculated as percentage of the dry sample weight to obtain an estimate of the organic matter content.

Samples for tephra analysis were ashed in a furnace at 550 °C for 2 hours and treated overnight with 10% HCl, prior to sieving at 80 and 25 μm . Sodium polytungstate was employed to separate the 2.3-2.5 g cm^{-3} density fractions (Turney 1998). Volcanic glass particles were identified by light microscopy and samples containing shards were then re-prepared for single-grain geochemical analysis. Shards were picked using a micromanipulator, prepared on microprobe slides and embedded in epoxy resin. Different grades of silicon carbide paper

and 9, 6 and 1 μm diamond suspensions were used to prepare polished grain surfaces for microprobe analysis. Major element analysis was undertaken on seven shards using a Cameca SX100 with five wavelength dispersive spectrometers at the Tephrochronology Analytical Unit at the University of Edinburgh (Table S2). Operating conditions follow those in Hayward (2012).

Radiocarbon dating (C-1981 and C-2011), age model construction (C-2011) and core-to-core alignment

Unidentified aquatic mosses were used for radiocarbon dating the lower part of core C-1981 (Håkansson 1984), whereas leaves, buds, flowers, seeds, and catkin scales of terrestrial plants were selected from core C-2011 (Table 1). The selected plant remains were rinsed multiple times in deionized water, placed in pre-cleaned glass vials and dried overnight at 105 °C. Samples were dated at the 14Chrono Centre, Queen's University Belfast, where pretreatment and measurement followed the methodology described in Steinhorsdottir *et al.* (2013) and Muschitiello *et al.* (2015b).

The age-depth model for core C-2011 was constructed with *OxCal4.2* (Bronk Ramsey 2010) and is based on 37 AMS ^{14}C dates (Table 1) calibrated with the IntCal13 calibration curve (Reimer *et al.* 2013). In addition, the published age of the Häseldalen tephra (Muschitiello *et al.* 2015b; Ott *et al.* 2016), identified at 508-509 cm depth (see below), was included in the age model. The sequence of ^{14}C dates was modelled multiple times prescribing different prior information parameters until the optimal set up was achieved. Since Bayesian age-depth modelling with OxCal mainly relies on the correct choice of k (Bronk Ramsey 2008), we performed several runs using different k parameters until satisfactory agreement indices (Bronk Ramsey 2009) were obtained. The Outlier_Model analysis was performed with the general setting and the prior probability fixed to 0.05, which weighs down the radiocarbon measurements that have a statistical probability of more than 5% of being outliers (Bronk Ramsey 2009). The final model was run using a k value of 0.4, suitable to constrain ^{14}C data in a flexible fashion (Blockley *et al.* 2008). The output resulted in a coherent age model with an overall solid structure of the dated sequence as defined by an overall good agreement index of 71.4% (Bronk Ramsey 2009).

To assign the chronology and age-model of core C-2011 to the pollen stratigraphy of core C-1981 (Björck and Liedberg-Jönsson, unpublished), we used a Monte Carlo algorithm for core-to-core stratigraphic alignment based on proxy records (Muschitiello *et al.* 2015a, b; Wohlfarth *et al.* 2017). This method leans upon a nonlinear deformation of the entity of one record onto a reference record via a Monte Carlo technique that delivers a suite of possible alignments

between the records and an optimal correlation. We applied this method using the LOI data of C-1981 and C-2011, and C-2011 as a target.

Pollen (C-1981), plant macrofossil and chironomid (C-2011) analyses

32 samples (1 cm³) from core C-1981 had already been prepared and analysed for pollen by Björck and Liedberg-Jönsson (unpublished) in accordance with the method described in Berglund & Ralska-Jasiewiczowa (1986). Larger *Betula pubescens*-type and smaller *Betula nana*-type pollen had been separated based on their size (Björck and Liedberg-Jönsson, unpublished). The pollen diagram for C-1981 was constructed using the program C2 of Juggins (2007). Local pollen assemblage zones were visually identified based on major changes in herb/grass (*Artemisia*, *Rumex*, *Filipendula*, Poaceae), shrub (*Hippophaë*, *Juniperus*, *Empetrum*) and tree (*Betula*, *Pinus*) pollen percentages.

181 samples for plant macrofossil analysis (sample size: 100-300 mL) extending between 748-542 and 518-456 cm depth were sieved under running water using a 150-µm mesh and the residue was examined under a stereomicroscope. All remains were counted and identified to as low taxonomic levels as possible. The plant macrofossil diagram was visually divided into three zones, of which zone two was further divided into three subzones, based on variations in species assemblages and their environmental and ecological implications.

185 samples for fossil chironomid analysis (sample size: ~ 5 g of dried sediment) (extending between 741 and 500 cm) were prepared applying standard methods (Brooks *et al.* 2007). The wet sediment was sieved through a 100-µm mesh and the residue was examined under a stereomicroscope. Larval head capsules were extracted with fine forceps and mounted permanently on microscope slides. Identification was performed under a light microscope. The minimum chironomid head capsule number per sample was set to 50 (Heiri & Lotter 2001). Constrained unweighted pair-group average (UPGMA) cluster analysis (chord distance) was employed to group the samples into four local faunal zones. De-trended correspondence analysis (DCA) was used to detect variance in the chironomid assemblages. DCA was run with square-root species transformation and down weighting of rare species.

Quantitative temperature reconstructions

The quantitative macrofossil-based minimum mean July air temperature reconstruction for C-2011 follows the procedure introduced in Väliranta *et al.* (2015), where a more detailed description is available. The reconstruction is based on an extensive meteorological and modern plant-distribution data set, which combines information on modern plant species distribution limits

(Lampinen *et al.* 2014) and measured daily mean July temperatures (1970–2000) (Venäläinen *et al.* 2005) from the same grid cells in Finland. The plant distribution database can therefore be used to correlate modern species distribution with climate variables, as it is based on continuous botanical surveys. For our minimum mean July temperature reconstruction, we however excluded plant species that have specific soil requirements. As a first step, we selected the most indicative plant species from the macrofossil assemblages (e.g., *Potamogeton berchtoldii*, *P. filiformis*, *P. compressus*, *Callitriche hermaphroditica*, *Nymphaea* sp., and *Typha*). In a second step, observations on modern plant species distribution (Lampinen *et al.* 2014) and mean July temperatures derived from the same grid cells were combined to estimate current species-specific July temperature requirements. The reconstructed July temperature value is a median value calculated over 5-6 observations along the northernmost distribution limit of the respective plant species. The same approach was also employed for the pollen assemblages of core C-1981, for which sparse pollen of *Typha* and *Myriophyllum spicatum* had been noted.

The chironomid-based mean July surface water temperature reconstruction used the expanded Fennoscandian calibration model (weighted-averaging partial least squares, WA-PLS) combining several data sets (Luoto *et al.* 2016). Since July water temperatures in the lakes of the training set closely track July air temperatures, the site-specific gridded air temperature data was directly used as water temperature values. The temperature gradient in the training set varies from 7.9 to 17.6 °C and encompasses subarctic, boreal and temperate lakes. The 2-component model currently includes 180 lakes and 129 taxa having an r^2_{jack} of 0.86, a root mean squared error of prediction (RMSEP) of 0.85 °C and a maximum bias of 0.75 °C. Sample-specific errors (eSEP) were estimated using bootstrapping cross-validation (999 iterations). Using the modern analogue technique (MAT), the cut-level of the 5th percentile of all chi²-distances in the modern calibration data were determined. These distances were then compared to the distance between each fossil assemblage and its most similar assemblage in the modern dataset and used to define ‘no close’ analogues.

Total organic carbon, carbon isotope, lipid biomarker and hydrogen isotope analysis (C-2011)

234 contiguous freeze-dried sub-samples (extending between 736 and 500 cm depth) were analysed for total organic carbon (TOC) and stable carbon isotopes ($\delta^{13}\text{C}$). Analyses were made at the Stable Isotope Laboratory, Department of Geological Sciences, Stockholm University using a Carlo Erba NC2500 elemental analyser coupled with a Finningan MAT Delta + mass spectrometer. The samples were treated with 2N HCl prior to analyses and the relative error for these

measurements was <1%. Isotope values are given in the conventional delta notation as ‰ deviation from the standard gas; the standard deviation for replicate measurements is less than 0.2‰.

Lipid extraction was performed on 188 samples (extending between 724 and 500 cm depth) with variable volume (2-8 cm³) after sonication with dichloromethane:methanol (9:1) for 20 minutes and subsequent centrifugation. The process was repeated three times and supernatants were combined. Aliphatic hydrocarbon fractions were isolated from the total lipid extract using silica gel columns (5% deactivated) that were eluted with pure hexane. Subsequently, a saturated hydrocarbon fraction was obtained by elution through 10% AgNO₃-SiO₂ silica gel using pure hexane as eluent. The saturated hydrocarbon fractions were analysed by gas chromatography - mass spectrometry for identification and quantification, using a Shimadzu GCMS-QP2010 Ultra. C₂₁ to C₃₃ *n*-alkanes were identified based on mass spectra from the literature and retention times. The concentration of individual compounds was based on the comparison of peak areas relative to that of an internal standard (squalane) that was added to the samples before total lipid extraction.

Hydrogen isotope ratios were determined at the Delta Facility, Stockholm University, using a Thermo Finnigan Delta XL mass spectrometer and all analyses were performed in triplicate. A standard mixture of *n*-alkanes with known δD composition (mix A4, provided by A. Schimmelmann, Indiana University, USA) was run several times daily to calibrate the measured δD values (‰) to VSMOW. For data interpretation, we only used sample values that were characterised in the isotope-ratio mass spectrometer chromatograms by baseline separated peaks, and also were of high enough peak size to fall within the linearity range of the instrument.

Results and Interpretation

Lithostratigraphy, LOI (C-2011, C-1981) and tephra (C-2011)

The basal sediments in core C-2011 (750-702 cm) are composed of alternating layers of fine sand, silt and clayey silt with distinct moss horizons and LOI values of <3% (Table S1, Fig. 2A). The overlying gyttja silts (702-664 cm) are characterised by slightly higher LOI values of 3-7%. LOI values increase continuously from 8% to around 35% in the clayey silty gyttja (664-613.5 cm) and silty gyttja (613.5-590 cm), but decline again in the silty gyttja/algae gyttja (590-582.5 cm) to slightly below 30%. The overlying algae gyttja (582-5-549 cm) has initial LOI values of up to 40%, but these decrease gradually and reach values of around 20% in the upper part of the silty gyttja (549-511.5 cm) (Fig. 2A). The sharp upper boundary of the silty gyttja at 511.5 cm indicates a

disturbance. LOI values increase again distinctly in the fine detritus gyttja (510-462 cm) and coarse detritus gyttja/peat (462-402 cm) and reach 90% (Table S1, Fig. 2A).

The lowermost sediments of core C-1981 are made up of partly organic silts and sands (600-575 cm) with LOI values <3% (Table S1, Fig. 2B). LOI gradually increases to 15% in the overlying gyttja silt (575-542 cm) and silty gyttja (542-482 cm) and attains 30% in the fine detritus gyttja (482-444 cm). The upper part of C-1981 is characterised by silty gyttja (444-427 cm) with LOI values of 17-26% and fine and coarse detritus gyttja (427-380 cm) with LOI values reaching 90% (Table S1, Fig. 2B).

High contents of sand and silt and low organic matter content in the lowermost part of both cores suggest high run-off and high sedimentation rates. The gradually increasing organic matter content and higher LOI values in the middle part of the sequences point to higher aquatic productivity and probably also to less catchment run-off, whereas the decrease and subsequent lower organic matter content indicate a return to lower aquatic productivity and higher run-off. The marked rise in organic matter content and the composition of the uppermost sediments suggest a gradual infilling of the basin.

Tephra shard concentration was low in the analysed samples of core C-2011 (<4 shards per 0.5 gdw) and only one distinct peak of 29 colourless shards was found at 508-509 cm depth (ATK 508-509) (Fig. 2A). Electron microprobe analysis of seven of these shards revealed a rhyolitic composition, likely an Icelandic origin and a geochemistry that shows strongest affinity to the Hässeldalen tephra (Davies *et al.* 2003; Lind & Wastegård 2011; Lane *et al.* 2012a; Housley *et al.* 2013; Larsen & Noe-Nygaard 2014; Wulf *et al.* 2016) with SiO₂ values >78 wt%, FeO_t values between 0.9-1.28 wt%, CaO values <0.72 wt% and a mean K₂O value of 3.66 wt% (Fig. 3, Table S2). Minor offsets however exist between the published data sets and ATK 508-509 since three of the shards fall outside the typical ranges of the K₂O and CaO values for the Hässeldalen tephra (Fig. 3). This may reflect differences in instrumental set-up or that the small number of shards analysed does not fully capture the full range seen at other sites. The stratigraphic position of ATK 508-509 seems however consistent with its occurrence in other sites. We therefore, correlate this tephra to the Hässeldalen Tephra.

Age-depth model and core-to-core alignment (cores C- 2011 and C-1981)

The age-depth model for core C-2011 exhibits a solid structure and appears robust (Fig. 4A). OxCal 4.2 treated only few samples as outliers (Ua-28101; Ua-29586; Ua-29596) (Table 1) and suggests that 732.5-503.5 cm depth corresponds to the time interval between 15.3 and 11.35 cal. ka BP (median

ages). The 95% error margin of the median modeled ages is 145-230 years between 732-662 cm, 100-130 years between 661-647 cm, 120-200 years between 646-612 cm and 80-160 years between 611-543 cm (Fig. 4A). The error increases distinctly between 540-510 cm due to a lack of suitable terrestrial plant remains for ^{14}C dating. We therefore regard the age-model between 540 and 510 cm (12.52-11.53 cal. ka BP) as uncertain. The scarcity of terrestrial plant macro remains below 735 cm and above 503 cm depth (Table 1) moreover prevents a direct age assignment for this part of the record. For the upper- and lowermost parts, which are not covered by the age model, we used deposition rates of 11 a cm^{-1} between 732.5 and 700.5 cm and of 25 a cm^{-1} between 509.5 and 503.5 cm, respectively to obtain estimated ages.

The LOI curves of C-1981 and C-2011 have a different temporal resolution, but display similar features, which allows for a good match between the two cores (Fig. 4B). The core-to-core alignment suggests that the interval between 600-385 cm depth in C-1981 corresponds to a depth of between 749-450 cm in C-2011 (Fig. 5B). Since the age model for C-2011 only extends between 732.5-503.5 cm or 15.3-11.4 cal. ka BP, corresponding to 600-425 cm depth in C-1981 (Fig. 4A), no ages can be assigned to the upper part of C-1981 (420-385 cm). The core alignment moreover suggests a 900 year-long hiatus between 445-440 cm since modelled ages change from 12.9 cal. ka to 12 cal. ka BP within 5 cm. This hiatus prevents us from assigning an age to the boundary between local pollen zones ATK-6 and ATK-5 (see below).

Pollen stratigraphy (core C-1981) and regional vegetation reconstruction

ATK-1 (600-565 cm; 15.3-14.6 cal. ka BP). – *Artemisia* pollen percentages are high, *Hippophaë* and *Juniperus* pollen occur in low numbers and *Empetrum* has a small peak (Fig. 5). The pollen assemblage suggests open vegetation dominated by herbs/grasses and shrubs. Correlations to the pollen assemblage zones established for Håkullsmosse and Björkeröds mosse on Kullen Peninsula (Berglund & Ralska-Jasiewiczowa 1986; Liedberg-Jönsson 1988) (Fig. 1A, B) are difficult, but based on high values for *Artemisia*, we tentatively correlate ATK-1 to Bj-1 and Bj-2 in Björkeröds mosse and to a regional pre-Bølling pollen zone (Liedberg-Jönsson 1988) (Fig. 5).

ATK-2 (565-507 cm; 14.6-14.1 cal. ka BP). – *Artemisia* pollen percentages are initially high, but decrease subsequently; *Hippophaë* and *Empetrum* pollen occur in low numbers, whereas *Juniperus* pollen increase; Cyperaceae have a distinct peak in this zone and *Rumex* a peak in the middle of the zone. *Betula pubescence* – type pollen percentages gradually increase towards the upper zone boundary. Single pollen of *Typha latifolia* occur at 562 cm (14.55 cal. ka BP) and of *Myriophyllum spicatum* between 535-528 cm (ca. 14.2 cal. ka BP). *Pediastrum coenobia* attain highest numbers (Fig. 5). The overall high frequencies of

herb/grass and shrub pollen suggest continued open vegetation, although the increase in *Betula pubescence* - type pollen percentages could indicate local presence. Based on the rise of *Juniperus* and slightly higher values for *Hippophaë* we correlate ATK-2 to pollen zone Bj-3 in Björkeröds mosse and to zone HÅM-1/HÅ-3 in Håkullsmosse (Berglund & Ralska-Jasiewiczowa 1986; Liedberg-Jönsson 1988), both assigned to the regional Bølling pollen zone (Liedberg-Jönsson 1988) (Fig. 5).

ATK-3 (507-495 cm; 14.1-13.9 cal. ka BP). – Poaceae and *Artemisia* pollen values increase markedly, *Empetrum* and *Juniperus* pollen occur in low numbers and tree pollen values decrease. Single pollen grains of *Myriophyllum spicatum* were observed (Fig. 5). Higher frequencies of herb/grass and shrub pollen suggest open vegetation and resemble those of zone HÅM-2/HÅ-4 in Håkullsmosse and zone Bj-4 in Björkeröds mosse (Berglund & Ralska-Jasiewiczowa 1986; Liedberg-Jönsson 1988), both of which have been assigned to the regional Older Dryas pollen zone (Liedberg-Jönsson 1988) (Fig. 5).

ATK-4 (495-461 cm; 13.9-13.1 cal. ka BP). – Cyperaceae, Poaceae and *Artemisia* pollen values are low, while tree and shrub pollen values increase and *Pediastrum coenobia* decrease again (Fig. 5). Lower pollen percentages for herbs/grasses and higher values for shrubs and trees suggest that shrubs and trees regionally increased and that open forests could have been present. Zone ATK-4 shows a good correlation with zones HÅM-3/HÅ-5 and HÅM-4/HÅ-6 in Håkullsmosse, whereas a correlation to Björkeröds mosse ((Berglund & Ralska-Jasiewiczowa 1986; Liedberg-Jönsson 1988) is not obvious. Local pollen zones HÅM-3/HÅ-5 and HÅM-4/HÅ-6 have been assigned to the early part of the regional Allerød pollen zone (Liedberg-Jönsson 1988) (Fig. 5).

ATK-5 (461-444 cm; 13.1- ? cal. ka BP). – *Juniperus*, *Empetrum* and *Filipendula* pollen percentages increase, tree pollen percentages are still high, but decline and *Artemisia* values remain low. *Pediastrum coenobia* again increase in numbers and single pollen grains of *Myriophyllum spicatum* occur (Fig. 5). The decrease in tree pollen values, generally lower grass/herb pollen and the increase in *Juniperus*, *Empetrum* and *Filipendula* suggest re-expansion of light-demanding species. The peak in *Juniperus* pollen percentages compares well to zone HÅM-5/HÅ-6 in Håkullsmosse (Berglund & Ralska-Jasiewiczowa 1986; Liedberg-Jönsson 1988). In comparison with Håkullsmosse, zone ATK-5 is therefore correlated to the later part of the regional Allerød pollen zone (Liedberg-Jönsson 1988) (Fig. 5).

It is important to note that the transferred age model indicates a ~ 900-year long hiatus between 445 cm (12.9 cal. ka BP) and 440 cm (12 cal. ka BP) depth (see above). This prevents assigning an age to the boundary between ATK-5 and ATK-6.

ATK-6 (444-427 cm; ? -11.5 cal. ka BP). – *Artemisia* has a distinct peak, Cyperaceae and Poaceae frequencies are high and *Betula pubescence* – type pollen, as well as *Juniperus* and *Empetrum* pollen decline markedly (Fig. 5). *Pediastrum* coenobia are low in numbers. High *Artemisia* frequencies throughout suggest open vegetation. The pollen assemblages resemble those of zones HÅM-6/HÅ-8 and HÅM-7/HÅ9 in Håkullsmosse (Berglund & Ralska-Jasiewiczowa 1986; Liedberg-Jönsson 1988), which have been attributed to the regional Younger Dryas pollen zone (Fig. 5).

ATK-7 (427-412 cm; <11.5 cal. ka BP). – *Artemisia* pollen decline, *Juniperus* and later *Empetrum* and *Filipendula* pollen values increase. *Typha latifolia* pollen appear and *Myriophyllum spicatum* pollen occur in the uppermost samples (Fig. 5). *Pediastrum* coenobia again increase in numbers. The increase of *Juniperus* and *Empetrum* pollen values marks the start of the Holocene in south Swedish pollen diagrams (Björck *et al.* 1996) and compares to pollen zone HÅM-8/HÅ-10 in Håkullsmosse (Berglund & Ralska-Jasiewiczowa 1986; Liedberg-Jönsson 1988) (Fig. 5).

Plant macrofossil assemblages (core C-2011) and local vegetation reconstruction

Zone I (744.5-675 cm; 15.45-14.55 cal. ka BP). – Well-preserved aquatic bryophytes, such as *Warnstorfia exannulata*-group and *Scorpidium scorpioides*, as well as *Chara* or *Nitella* oospores were abundant (Fig. 6). Few *Carex* sp., *Juncus/Luzula* and *Cerastium semidecandrum/glomeratum* - type seeds were found, but species-level identification of the latter was not possible. *Salix polaris* leaves are present throughout, which suggest that *Salix* was locally present.

Zone IIa (675-620 cm; 14.55-13.64 cal. ka BP). – The abundant vascular aquatic plant assemblages comprise *Ranunculus* sect. *Batrachium*, various *Potamogeton* species and *Myriophyllum* (Fig. 6). Herb remains include *Equisetum*, *Carex* sp. and *Juncus/Luzula* and sparse finds of *Potentilla* sp. and *Cerastium semidecandrum/glomeratum* – type. Woody plants comprise *Dryas octopetala*, *Salix* sp., *S. polaris*, *Betula* sp. and *Betula nana*. Noteworthy are finds of two seeds of tree *Betula* in one sample. Together, these plant assemblages suggest that the vegetation cover had become denser and that tree birch was present close to the lake.

Zone IIb (620-542 cm; 13.64-12.57 cal. ka BP). – Aquatic remains include fairly large numbers of *Cristatella* and *Chara/Nitella* and various vascular plants, such as *Ranunculus* sect. *Batrachium*, *Potamogeton alpinus* – type, *P. compressus*, *Myriophyllum*, *Callitriche* cf. *hermaphroditica* and *Nymphaea* sp. (Fig. 6). Herb remains are scarce, whereas woody plant remains (e.g., *Dryas octopetala*, *Salix* sp., *Betula* sp. and *Betula nana*) are more frequent. In addition to tree *Betula*, of which several seeds and catkin scales have been found, we also detected *Pinus sylvestris* needles and conifer bark in one sample (555 cm depth; 12.8 cal. ka BP).

Together, these finds provide evidence that tree *Betula* and conifer trees had colonized the surroundings of the lake. A prominent feature is also the increase in fire frequency as testified by macroscopic charcoal between 575-542 cm (12.97-12.57 cal. ka BP), which shows presence of fire-sensitive woody plants and dry conditions. Abundant *Cenococcum* sclerotia moreover indicate the development of catchment soils and soil erosion.

Zone IIc (518-505 cm; 11.77-11.38 cal. ka BP). – The four analyzed samples contained some bryophytes, *Chara/Nitella* oospores, scarce seeds of *Ranunculus* sect. *Batrachium*, *Potamogeton berchtoldii/filiformis*, *Potamogeton* sp. and *Potentilla* sp., few remains of *Betula* sp. and *B. nana* as well as *Cenococcum* sclerotia (Fig. 6). The sparse plant remains suggest a return to an open vegetation and the occurrence of *Cenococcum* sclerotia in the upper part of the zone indicates soil erosion.

Zone III (505-450 cm; 11.38-10.01 cal. ka BP). – The amount and diversity of aquatic plant remains increase distinctly (e.g. various *Potamogeton* species, *Myriophyllum*, *Callitriche* cf. *hermaphroditica*, *Nymphaea* sp.) as compared to the previous zones, suggesting a change in lake status. Scarce finds of terrestrial plants include seeds of *Typha*, *Comarum palustre*, *Menyanthes trifoliata*, *Salix* sp., *Betula* sp. and *Betula nana*. Remains of tree *Betula* and *Pinus sylvestris* are now more frequent (Fig. 6). The terrestrial plant assemblages thus show that tree birch and conifers were present around the lake. Higher numbers of charcoal particles in the lower part of the zone moreover indicate frequent fires and probably drier conditions.

Chironomid assemblages and lake status changes (core C-2011)

Zone I (740.5-682.5 cm; 15.40-14.68 cal. ka BP). – *Micropsectra radialis*-type and *Pseudodiamesa* dominate and *Corynocera oliveri*-type chironomids are common. *Hydrobaenus lugubris*-type, *Orthocladus* (*P.*) *consobrinus*-type and *Paratanytarsus austriacus*-type increase towards the upper part of the zone (Fig. 7). These taxa indicate a subarctic to high arctic fauna and oligotrophic lake water conditions.

Zone II (682.5-664.5 cm; 14.68-14.32 cal. ka BP). – Taxa that are abundant in zone I disappear or decrease and new dominating taxa are *Psectrocladius sordidellus*-type, *Chironomus anthracinus*-type and *Paratanytarsus penicillatus*-type (Fig. 7). The chironomid assemblages in zone II are associated with aquatic vegetation, which suggests higher lake organic productivity.

Zone IIIa (664.5-560.5 cm; 14.32-12.86 cal. ka BP) and IIIb (560.5-515 cm; 12.86-11.68 cal. ka BP). – Taxa that characterized zone II decrease and *Corynocera ambigua* dominates (Fig. 7). *Microtendipes pedellus*-type dominates in zone IIa and *P. sordidellus*-type, *Sergentia coracina*-type and *O. consobrinus*-type increase in zone IIb. *C. ambigua* and *Microtendipes* are characteristic in

boreal forest lakes and become typically abundant when lake environmental conditions change. The increase of *Sergentia coracina*-type chironomids suggests a decrease in hypolimnetic oxygen, as these taxa possess hemoglobin, which enables them to tolerate temporary anoxia.

Zone IV (515-496.5 cm; 11.68-11.18 cal. ka BP). – *C. ambigua* remains dominant and *M. pedellus*-type increases again, while taxa that were common in zone III disappear or decrease (Fig. 7). The chironomid fauna is typical for oligo-mesotrophic boreal forest lakes.

Summer temperature reconstructions

The minimum July temperature estimates derived from indicator plant species primarily relies on the occurrence of seeds (C-2011) and to some extent also on the presence of pollen (C-1981).

Cerastium semicandrum currently has its main distribution area in the southern boreal/temperate bio-climatic zone, which corresponds to July temperatures >16 °C. However, small populations also occur north of the main population, thus a cautious minimum July air temperature reconstruction is >13 °C (Table 2). The occurrence of seeds of *Cerastium semidecandrum/glomeratum* – type between 15.45 and 14.55 cal. ka BP in C-2011 (Fig. 6) could therefore indicate that minimum mean July air temperatures were >13 °C. However, since species-level identification was not possible, we refrain from assigning summer temperatures to this part of our record. The occurrence of *Potamogeton berchtoldii/filiformis* – type between 14.55-13.64 cal. ka BP points to minimum mean July temperature requirements of 12-13.5 °C and the presence of *Callitriche hermaphroditica* and *Potamogeton compressus* between 13.64 and 12.57 cal. ka BP suggests an increase in minimum mean July air temperatures to around 14 °C (Table 2, Fig. 6). Seeds and leaves of *P. berchtoldii/filiformis*- type, *P. berchtoldii*, *Callitriche hermaphroditica* and *Nymphaea* sp. after 11.38 ka cal. BP (Fig. 6) show that minimum mean July air temperatures attained around 13.5 °C (Table 2).

Single pollen grains of *Typha latifolia* in C-1981 at 14.55 cal. ka BP point to minimum mean July temperatures of 15-16 °C and *Myriophyllum spicatum* pollen found between 14.45-13.88 and at 12.98 cal. ka BP suggest minimum mean July temperatures of 12 °C (Table 2, Fig. 5). The continuous occurrence of *Typha latifolia* pollen after 11.5 cal. ka BP in turn indicates a rise in minimum mean July temperatures to 15-16 °C (Table 2, Fig. 5).

The chironomid-based temperature model used here was calibrated against summer air temperature measurements. However, since it is known that chironomids respond more sensitively to summer water temperature, especially

in glacier/snowmelt fed sites (Luoto & Nevalainen 2013), we here interpret our chironomid-based temperature reconstruction as summer water temperature changes. Four of the 123 samples used for chironomid analysis had poor modern analogues, but otherwise the assemblages had a good match in the training set. All poor analogue samples (690.5, 684.5, 682.5 and 680.5 cm) were situated close to the boundary of zones I and II (Fig. 7). Chironomid-inferred mean July surface water temperatures vary between 6 and 15 °C. Coldest reconstructed temperatures occur in zone I (740.5-682.5 cm; 15.40-14.68 cal. ka BP). Zones II and IIIa are characterized by warm, but oscillating July surface water temperatures (682.5-560.5 cm; 14.68-12.86 cal. ka BP) and zone IIIb by a progressive decrease in temperatures (560.5-515 cm; 12.86-11.68 cal. ka BP). In zone IV (515-496.5 cm; 11.68-11.18 cal. ka BP) reconstructed July surface water temperatures increase again. The reliability of our chironomid-based temperature reconstruction is supported by the strong correlation between chironomid-inferred temperatures and the primary DCA axis 1 scores ($R = 0.94$, p -value = <0.001), whereas no significant correlation was found between the inferred temperatures and the secondary DCA axis 2 scores ($R = 0.14$, p -value = 0.135)

Geochemistry (core C-2011)

TOC, which is here used as a proxy for lake organic productivity, together with LOI (Fig. 2A) has values of $<5\%$ in the lower part of the record (735-661 cm; 15.36-14.26 cal. ka BP) and of around 5% between 660 and 625 cm (14.25-13.73 cal. ka BP) (Fig. 8). A first gradual rise to 20% occurs between 625 and 600 cm (13.73-13.30 cal. ka BP). Stable values of around 20% are followed by slightly lower values (592-582 cm; 13.18-13.02 cal. ka BP) and by a renewed rise to 25% (582-567 cm; 13.02-12.90 cal. ka BP) (Fig. 8). Thereafter TOC values decline gradually to around 10% and only start to rise again at 510 cm (11.52 cal. ka BP) to attain 30% at 503 cm (11.35 cal. ka BP). The general pattern of the TOC curve is similar to that of the LOI curve (Fig. 2A), suggesting low aquatic productivity and/or high run-off in the basal part (15.36-13.73 cal. ka BP) and higher aquatic productivity/less run-off in the middle (13.73-12.90 cal. ka BP) and uppermost parts (>11.52 cal. ka BP). Lower TOC values between 540 and 510 cm (12.51-11.52 cal. ka BP) indicate that aquatic productivity had decreased (Fig. 8).

Conservative lithogenic elements (e.g., K, Si, Ti, Rb), which are indicative of minerogenic input, generally compare well with the lithostratigraphy and show an inverse relationship with the TOC curve. These elements have overall higher values in the sand and silt-rich units in the basal part of the record and lower values in organic-rich layers (582.5-550 and 510-500 cm; 13.03-12.70 cal. ka BP and >11.52 cal. ka BP) (see Fig. S1). The potassium curve, which is here used as a representative for the silicate-hosted elements Si, Ti and Rb, displays

distinct peaks in the basal sand layers, minimum values between 582.5-562 cm (13.02-12.87 cal. ka BP) and higher values between 550-510 cm (12.71-11.52 cal. ka BP) (Fig. 8). These values reflect higher run-off, likely enhanced by scarce catchment vegetation and lack of catchment soils, more stable catchment conditions (13.02-12.87 cal. ka BP and <11.52 ka BP) and increased erosion between 12.71-11.52 cal. ka BP.

The $\ln(\text{Ca}/\text{Ti})$ ratio is a measure for changes in mineral input and lake and catchment productivity. While Ti is generally hosted in minerals like rutile, ilmenite and sphene or bound to clays (Nesbitt & Markovics 1997), Ca can be hosted in feldspars or carbonates, absorbed to organic matter, or precipitated in the water column as CaCO_3 (Wetzel 2001). The higher $\ln(\text{Ca}/\text{Ti})$ ratio in the basal part of the record, which is characterised by low TOC values and several sand layers, likely reflects changes in mineral material (Fig. 8). Alternating inputs of feldspars/sands and finer grained material could for example explain the relatively higher Ti content. The minor peak in $\ln(\text{Ca}/\text{Ti})$ between 675-665 cm depth (14.55-14.33 cal. ka BP) on the other hand coincides with constant K values (and constant mineral input) and therefore suggests an increase in lake and catchment organic productivity. The gradual rise in $\ln(\text{Ca}/\text{Ti})$ that starts at 620 cm (13.64 cal. ka BP), the more distinct increase between 582.5-549 cm (13.02-12.69 cal. ka BP) and the subsequent decrease (549-515 cm; 12.69-11.67 cal. ka BP) and rise (510 cm; >11.52 cal. ka BP) are mirrored by the TOC curve (Fig. 8). Together these proxies suggest gradually increasing aquatic productivity (13.64-12.69 cal. ka BP), a decline in aquatic productivity (12.69-11.67 cal. ka BP) and a renewed rise at 11.52 cal. ka BP.

$\delta^{13}\text{C}$ values fluctuate between -23 and -28‰ in the lower part of the record (735-672 cm; 15.36-14.48 cal. ka BP), increase markedly at 672 cm (14.48 cal. ka BP), remain around -20‰ until 625 cm (13.73 cal. ka BP) and decrease thereafter (Fig. 8). Stable values of around -22‰ between 615 and 592 cm (13.56-13.18 cal. ka BP) are followed by a gradual increase and highest values of -18‰ between 535-520 cm (12.35-11.84 cal. ka BP). The subsequent decrease to -22‰ is interrupted at 511-510 cm (11.55-11.52 cal. ka BP), where the lithology suggests sediment disturbance (Fig. 8). The marked shift from lower to higher values at 672 cm (14.48 cal. ka BP) compares well to the plant macrofossil data set (Fig. 6), which shows that terrestrial plant material dominates below 675 cm (14.55 cal. ka BP). Overall higher frequencies of aquatic plant remains between 675 and 450 cm (>14.55 cal. ka BP) are also well reflected in the $\delta^{13}\text{C}$ values.

The concentration of saturated C_{20} highly-branched isoprenoids (C_{20} HBI) displays a marked peak at 670 cm (14.43 cal. ka BP) and strongly fluctuating values and minor peaks in the middle and upper part of the record (Fig. 8). C_{20} HBI has been associated with the occurrence of the epiphytic diatom *Gomphonema acuminatum*, since Muschitiello *et al.* (2015a) found a good

correspondence between C₂₀ HBI concentrations and higher/lower percentages for this diatom species in south Swedish lateglacial lake sediments. Although *Gomphonema acuminatum* is present in a variety of habitats and on a variety of substrates, it is known to prefer standing water and to occur as a slimy cover on water plants. The marked increase in C₂₀ HBI concentrations at 670 cm (14.43 cal. ka BP) coincides with increasing numbers of aquatic plants (*Ranunculus* sect. *Batrachium*, *Potamogeton berchtoldii/filiformis* – type, *P. alpinus*) and overall higher concentrations thereafter are mirrored by abundant aquatic vegetation (Figs 6, 8). We therefore speculate that C₂₀ HBI concentrations at Atteköpsosse reflect the presence of diatom taxa that are attached to aquatic plants and that C₂₀ HBI is an indirect proxy for the available aquatic biomass.

n-C₂₃ alkane concentrations are low in the basal sediments, but start to increase at 700 cm (14.95 cal. ka BP) and reach >1000 ng g⁻¹ (TOC) at 665 cm depth (14.33 cal. ka BP) (Fig. 8). Concentrations fluctuate between 1000-2000 ng g⁻¹ (TOC) between 665-625 cm, but decline again to around 500-1000 ng g⁻¹ (TOC) between 625-565 cm depth (13.73-12.89 cal. ka BP). Higher concentrations of 1000-2000 ng g⁻¹ (TOC) between 565-510 cm depth (12.89-11.52 cal. ka BP) and a subsequent decline to around 500 ng g⁻¹ (TOC) characterise the upper part (Fig. 8). Fluctuations in the concentrations of these *n*-alkanes point to varying contributions of submerged macrophytes (Ficken *et al.* 2000; Aichner *et al.* 2010; Gao *et al.* 2011; Bush & McInerney 2013; Rach *et al.* 2014). In comparison with the plant macrofossil assemblages, we suggest that low concentrations of *n*-C₂₃ alkanes in the basal part are linked to a lower abundance of aquatic plant remains (Figs 6, 8). Higher *n*-C₂₃ alkane concentrations between 665-625 cm (14.33-13.73 cal. ka BP) correspond to the frequent occurrence of *Ranunculus* sect. *Batrachium* and *Potamogeton* spp., whereas lower concentrations between 625 and 565 cm (13.73-12.89 cal. ka BP) coincide with lower numbers of these taxa (Figs 6, 8). On the other hand, the rise in *n*-C₂₃ alkane concentrations between 565-550 cm depth (12.89-12.59 cal. ka BP) co-occurs with high abundances of *Chara/Nitella* remains (Figs 6, 8). The apparent high concentrations after 550 cm (12.59 cal. ka BP) however are an artefact of the declining TOC content. Moreover, the age model for this part of the record is not precise, which means that there is a high uncertainty regarding accumulation rates and calculated fluxes.

n-C₂₉ alkane concentrations, which represent higher terrestrial plants (Eglinton & Hamilton 1967; Rach *et al.* 2014), display a similar pattern as the *n*-C₂₃ alkane concentration curve, with low concentrations in the bottommost samples, a step-wise increase between 700-665 cm (14.95-14.33 cal. ka BP) and higher concentrations of around 1000-1500 ng g⁻¹ (TOC) between 665-650 cm (14.33-14.18 cal. ka BP) and between 635-625 cm (13.89-13.73 cal. ka BP). Concentrations of <500 ng g⁻¹ (TOC) are noted between 650-635 cm (14.18-13.89 cal. ka BP) and between 625-565 cm (13.73-12.89 ka BP) (Fig. 8). The

upper part (565-510 cm; 12.89-11.52 cal. ka BP) displays again a gradual rise in *n*-C₂₉ alkane concentrations to >1500 ng g⁻¹ (TOC), followed by a drop at 510 cm depth. However, as with the *n*-C₂₃ alkane record, the apparent higher concentrations after 550 cm (12.59 cal. ka BP) are biased by normalization against the TOC content and age model uncertainties. *n*-C₂₉ alkanes are found in a variety of higher terrestrial plant species and have for example been assigned to *Salix* sp., *Betula* sp. and grasses in the Lateglacial sediments of Holzmaar (Rach *et al.* 2014). Macrofossil remains of *Salix* sp. are present throughout at Atteköpsmosse and *Betula nana* and tree *Betula* are present after 14.55 ka BP (Fig. 6). None of these taxa show however a change in abundance when *n*-C₂₉ alkane concentrations decrease/increase. The discrepancy between *n*-C₂₉ alkane concentration and plant macrofossil abundance is not surprising since finds of plant macrofossil are often not continuous and often by chance. Absence of plant remains in sediments does not mean that these plants did not exist. Another explanation for the observed discrepancy could be related to a change in the relative contribution of aeolian-transported leaf waxes (either on leaves or ablated) and/or input of leaf waxes from eroded soil organic matter. Indeed, lowest/highest *n*-C₂₉ alkane concentrations generally correspond to intervals with decreased/increased erosion rates as indicated by TOC and lithogenic elements (Fig. 8).

Hydrological reconstructions

Hydrogen isotopes (δD) of aquatic- (δD_{aq}) and terrestrial-derived (δD_{terr}) lipid biomarkers have been used as indicators of local hydro-climate shifts controlled by moisture source composition, moisture pathway changes and condensation temperature (Sachse *et al.* 2004, 2012; Rach *et al.* 2014). Southern Sweden receives its moisture predominantly from the North Sea, but also from the Nordic Seas (Gustafsson *et al.* 2010). Changes in δD_{aq} and δD_{terr} values at Atteköpsmosse may thus provide information not only with respect to local hydro-climatic shifts, but also regarding changes in the isotopic composition of the precipitation source, such as shifts in sea surface and air temperatures.

The curves for δD *n*-C₂₃ (mainly aquatic macrophytes) (Ficken *et al.* 2000; Aichner *et al.* 2010) and δD *n*-C₂₉ (higher terrestrial plants) (Diefendorf *et al.* 2011) have similar patterns with strongly fluctuating values between 725-690 cm (15.23-14.82 cal. ka BP), step-wise rising values between 690-670 cm (14.82-14.43 cal. ka BP) and highest values between 670-625 cm (14.43-13.73 cal. ka BP) (Fig. 8). Values decline thereafter and range around -160 to -170‰ and -200‰, respectively. The δD *n*-C₂₃ (δD_{aq}) record also compares well to the δD of C₂₀ HBI, which represents diatoms and thus is an aquatic biomarker. This latter data set has not been completely analysed, has lower concentrations and consequently a greater error of measurement and appears therefore more

variable than the δD record of the n -C₂₃ alkanes (Fig. 8). The similarity between these two data sets provides however confidence that δD n -C₂₃ (δD_{aq}) purely reflects the source water and that it has not been influenced by changes in the composition of the aquatic macrophyte community, which can compromise the primary source water signal.

Although our δD records exhibit the same structure, it is apparent that the δD n -C₂₃ (δD_{aq}) curve has larger amplitudes than the δD n -C₂₉ (δD_{terr}) data set (Fig. 8). This could have been caused by several factors: i) More negative source water δD values, together with colder air temperatures concur with drier climatic conditions, which in turn leads to greater evapotranspiration and deuterium enrichment in terrestrial plants compared to surface lake water (Rach *et al.* 2014). The δD_{terr} signal would then reflect a muted source water signal. ii) Under warmer (colder) conditions, a longer (shorter) ice-free season causes lake water (but not groundwater) to become more enriched (depleted) in deuterium due to a different balance between precipitation and evaporation (Gibson 2002), an effect that does not affect soil water. This might explain the comparably lower δD n -C₂₃ (δD_{aq}) values between 12.9-11.5 cal. ka BP, but would also suggest a gradual lengthening of the ice-covered period prior to 12.9 cal. ka BP. iii) Lake water isotopic composition was to a stronger extent influenced by meltwater from seasonal or perennial snow, while terrestrial plants primarily used the precipitation falling during spring and summer. Changing winter precipitation regimes thereby impose a larger variability on δD_{lake} and δD_{aq} , as compared to δD_{terr} . Under such a scenario, the ancient Atteköpsmossen lake would for example have received more meltwater between 12.9-11.5 cal. ka BP.

Given the uncertainties surrounding the potential modulation of especially the lake water isotopic composition (ice cover, evaporative enrichment, changes in meltwater input), we refrain from using the isotopic difference between δD_{terr} and δD_{aq} ($\Delta\delta D_{terr-aq}$) as a proxy for catchment evapotranspiration and paleo-humidity (Rach *et al.* 2014). However, the good covariation between the δD n -C₂₃ (δD_{aq}) and δD n -C₂₉ (δD_{terr}) records (Fig. S2) supports a common origin, suggesting that the δD record can be interpreted as reflecting the source water region and/or temperature.

The strongly fluctuating δD n -C₂₃ (δD_{aq}) values between 725-690 cm (15.23-14.82 cal. ka BP), the subsequent step-wise increase and higher (less negative) values between 670-625 cm (14.43-13.73 cal. ka BP) thus suggest that an alternating fresher and saltier marine source of precipitation and/or colder and warmer conditions were followed by a shift to a predominantly saltier marine source of precipitation and/or warmer conditions between 14.5 and 13.7 cal. ka BP (Fig. 8). The decline in δD n -C₂₃ (δD_{aq}) values at 625 cm depth (13.73 cal. ka BP) and subsequent low values, especially between 615-595 cm (13.56-

13.21 cal. ka BP) and after 555 cm depth (12.79 cal. ka BP), accordingly point to a fresher marine source and/or colder conditions.

Discussion

Lake status and vegetation changes and summer temperature reconstructions

The oligotrophic lake that existed in the Atteköpsmosse basin before 14.7 cal. ka BP was characterised by high run-off, erosion and low aquatic productivity as shown by the presence of sand and silt layers, high values of lithogenic elements, low organic matter content, a subarctic to high arctic chironomid fauna and scarce aquatic plant remains (Fig. 9). The unstable catchment around the lake supported a fairly poor herb and shrub flora. Since the pollen and plant macrofossil data sets of Atteköpsmosse do not allow estimating minimum mean summer temperatures for this early time interval, we refer to the plant macrofossil assemblages of sites on Kullen Peninsula (Berglund & Ralska-Jasiewiczowa 1986; Liedberg-Jönsson 1988) to derive tentative minimum mean July temperatures of 16 °C (Table 3; Fig. 9). These values are considerably higher than lake surface water July temperatures (6-9 °C) reconstructed from Atteköpsmosse's chironomid assemblages (Fig. 9). Similar discrepancies between July lake surface (inferred from chironomids) and air temperatures (inferred from plants and coleoptera) have also been observed during the early lake stage (~14.1-14.2 cal. ka BP) at Hässeldala Port in southeast Sweden (Watson 2008; Wohlfarth *et al.* 2017) and have been linked to melting of local stagnant ice. With a deglaciation age of around 17 cal. ka BP for the west coast of southern Sweden (Sandgren & Snowball 2001; Hughes *et al.* 2016) (Fig. 1A) and a basal sediment age of 15.5 cal. ka BP for the Atteköpsmosse basin, it is likely that stagnant ice on Hallandsåsen only started to melt some 1500 years after the active ice sheet had disappeared. High summer temperatures, as indicated by climate indicator plants, led to enhanced melting of remnant ice and to increased run-off to the basin as evidenced by the deposition of mineral-rich sediments between 15.5-14.55 cal. ka BP (Fig. 9). The inflow of cold meltwater thus kept lake water temperatures colder than ambient air temperatures. This conclusion is in line with the study by Luoto & Nevalainen (2013), who showed that chironomid-based temperature reconstructions are influenced by lake-specific thermal conditions, such as for example cold water inflow from snowmelt and groundwater.

A first distinct environmental change is visible around 14.7 cal. ka BP, as chironomid assemblages indicate an increase in aquatic vegetation and a distinct rise in mean July lake surface water temperatures to 11-13 °C. This increase temporally coincides with the transition from Greenland Stadial (GS) 2.1a to Greenland Interstadial (GI) 1e (Fig. 9) and suggests that the ancient lake at Atteköpsmosse indirectly registered the large-scale climate shift that

characterised the transition between GS-2.1a and GI-1e. The temperature rise in the North Atlantic region across this transition (Steffensen *et al.* 2008) was likely the trigger for the subsequent marked environmental changes seen at Atteköpsmosse. Chironomid-inferred mean lake surface water July temperatures further rise to 13-15 °C at 14.5 cal. ka BP, lake organic productivity increases, aquatic plants become abundant and a variety of herbs, dwarf shrubs and shrubs now colonise the surroundings of the lake (Fig. 9). Denser vegetation cover, a stabilization of the catchment and a decrease in run-off can also be inferred from the sediment composition and the decrease in lithogenic elements. Together, these fairly stable environmental settings could have provided the necessary conditions for tree birch to colonise areas close to the lake, as evidenced by finds of seeds ~14.5 cal. ka BP (Fig. 9). Atteköpsmosse is however not the first site in southern Sweden, where macroscopic tree birch remains dating to the Bølling pollen zone have been found. The plant macrofossil data sets from Björkerödsmosse and Håkullsmosse on Kullen Peninsula (Liedberg-Jönsson 1988) (Table 3) and from Körslättamossen in southern Sweden (Hammarlund & Lemdahl 1994) show for example that tree birch was present during the Bølling pollen zone, and possibly even earlier. Atteköpsmosse's pollen and plant macrofossil data sets estimate minimum mean July temperatures of 12-13 °C, which are slightly below those reconstructed for the Kullen Peninsula sites (Table 3), but comparable to chironomid-inferred summer water temperatures (Fig. 9). The good correspondence between these temperature estimates implies that meltwater run-off had ceased and no longer influenced the chironomid assemblages. A further change is noticed around 14.3 cal. ka BP when the ancient lake changed into a boreal forest lake and aquatic productivity increased further. Chironomid assemblages now indicate fluctuating mean lake surface water July temperatures of between 11 and 15 °C (Fig. 9).

The cooling during the regional Older Dryas pollen zone (Berglund *et al.* 1994) and GI-1d is not registered in the Atteköpsmosse data set (Fig. 9). This is surprising given that several south Swedish lake sediment records suggest that climate conditions became cooler and drier during this time interval (Björck & Möller 1987). We therefore speculate that the sheltered location of Atteköpsmosse and its proximity to the ocean could have acted as a buffer.

Around 13.7-13.6 cal. ka BP the lake and its catchment experienced another series of changes (Fig. 9). The organic matter content now displays a more or less steady rise, which points to a continuous increase in lake aquatic productivity and/or decreased run-off; aquatic plant species are diverse and abundant and the catchment vegetation, which was still dominated by herb, dwarf shrub and shrub communities, also included tree *Betula* and *Pinus sylvestris*, as macroscopic finds of these appear by 13-12.8 cal. ka BP (Fig. 9). The presence of tree *Betula* during the Allerød pollen zone is not surprising, since its plant macrofossil remains have been reported from numerous sites in southern

Sweden (Liedberg-Jönsson 1988; Hammarlund & Lemdahl 1994) and Denmark (Mortensen *et al.* 2011, 2014; Fischer *et al.* 2013). The early occurrence of *Pinus sylvestris* is however surprising since macroscopic finds of this tree species have never before been reported from Lateglacial sediments in southern Sweden or Denmark (Mortensen *et al.* 2014). *Pinus* pollen percentages of 50-85% have earlier been described for the Allerød pollen zone from several Lateglacial sites in Blekinge, southeastern Sweden, and based on these it has been suggested that *Pinus* may actually have been present in the landscape (Björck 1981). Yet, it could be argued that these high pine pollen percentages are due to long-distance transport from, for example northern Germany, from where *Pinus* logs dating to the Allerød have been reported (Terberger *et al.* 2004).

The *Pinus* needle bud scales found in the Atteköpsmosse sediments (Fig. 6) occur during a time interval when major elements indicate stable catchment conditions and chironomid assemblages typical for boreal forest lakes are present. Moreover, the distinct increase in charcoal particles during the upper part of the Allerød pollen zone (Figs 6, 9) indicates frequent forest fires and provides indirect evidence for the availability of fire sensitive woody plants (such as *Pinus*). The *Pinus* finds also co-occur with *Cenococcum* sclerotia, which not only suggest the development of catchment soils, probably in connection with an early tree establishment, but also indicate soil erosion. The remains of Allerød pine trees that were growing in the catchment could therefore easily have been transported into the lake basin. These various proxies provide indirect support for the presence of *Pinus* in the lake's catchment. Therefore, it seems unlikely that the pine macrofossils in Atteköpsmosse's late Allerød sediments were reworked from glacial diamictos and/or are due to contamination by Holocene sediments during the coring procedure (see Methods section). Based on the arguments outlined above, we also hypothesise, based on the reported high *Pinus* pollen percentages, that *Pinus sylvestris* was present in other areas in southern Sweden, possibly in sheltered, favourable sites.

The plant communities point to minimum mean July temperatures of around 14 °C throughout the Allerød pollen zone, which is in good agreement with the temperature reconstructions using chironomid assemblages. These values also compare well to minimum mean July temperatures derived from plant indicator species in Björkerödsmosse and Håkullsmosse (Liedberg-Jönsson 1988) (Table 3; Fig. 9).

Interestingly, the organic matter content of the sediments decreases between 13.2-13 cal. ka BP and then increases to high values between 13-12.9 cal. ka BP. None of the other proxies, however registers these changes, except for charcoal, which was present in very low numbers earlier and which increases distinctly at 12.9 cal. ka BP. A similar peak in organic matter content has been discussed for the site of Hässeldala Port in Blekinge (Wohlfarth *et al.* 2017) and has also been reported for other Lateglacial records in southern Sweden (Björck

& Möller 1987; Berglund *et al.* 1994). A combination of different proxies led Wohlfarth *et al.* (2017) to suggest that Hässeldala Port experienced drier and colder conditions at that time. This led to a lake level lowering and to an expansion of the aquatic vegetation, which in turn increased deposition of organic matter and raised the nutrient level in the ancient Hässeldala lake. The marked increase in charcoal at Atteköpsmosse (Figs 6, 9), which coincides with a rise in organic matter content, could indeed suggest the start of dry conditions.

Just after the peak in organic matter content, at 12.85 cal. ka BP, mean lake surface water July temperatures drop to around 12 °C. This distinct temperature shift temporally coincides with the start of GS-1 (Fig. 9). The chironomid fauna is still typical for boreal forest lakes and plant macrofossil assemblages and thereof inferred minimum mean July temperatures display no major changes, while lake aquatic productivity gradually decreases. By 12.5 cal. ka BP organic matter values are again similar to those at around 13.6-13.7 cal. ka BP and suggest an increase in erosion/run-off and lower aquatic productivity. In contrast to several sites in southern Sweden (Liedberg-Jönsson 1988) and Denmark (Bennike *et al.* 2004; Mortensen *et al.* 2011), no remains of tree birch were found in Atteköpsmosse's Younger Dryas sediments. This is likely due to the lack of plant macrofossil samples between 12.6-11.8 cal. ka BP (Fig. 9).

Chironomid-inferred mean lake surface water July temperatures drop to below 10 °C around 12.3 cal. ka BP and remain low until around 11.65 cal. ka BP (Fig. 9). A similar two-step decrease in chironomid-inferred temperatures has been noted in Hässeldala Port (Wohlfarth *et al.* 2017) and in Scottish Lateglacial sites (Walker & Lowe 2017) and could suggest more severe climate conditions during the later part of Younger Dryas. Plant indicator species based minimum mean July temperatures derived from the Kullen Peninsula sites (Liedberg-Jönsson 1988) on the other hand remain around 14 °C throughout the Younger Dryas (Table 3, Fig. 9) and thus suggest significantly higher July temperatures.

The transition into the Holocene is first documented by a distinct change in chironomid assemblages and a rapid increase in lake water July temperatures from 10 to 14 °C, which are followed by increasing aquatic productivity and stable catchments (Fig. 9). The appearance of *Typha* pollen in Atteköpsmosse just after 11.5 cal. ka BP suggests minimum mean July temperatures of 16 °C, which compares well to values estimated using the Kullen Peninsula plant macrofossil records (Table 3, Fig. 9). Atteköpsmosse's plant macrofossil assemblages however display no change until a few hundred years later, when aquatic plants become abundant again and tree birch and *Pinus sylvestris* recolonised the surroundings of the ancient lake. Abundant charcoal around 11.4 cal. ka BP suggests dry conditions and availability of fire sensitive woody plants and perhaps also of litter.

Hydro-climate history and implications

The δD_{aq} record, which is here used as a proxy for changes in the isotopic composition of the marine moisture source and/or condensation temperature (Rach *et al.* 2014; Muschitiello *et al.* 2015b), shows large variability before 14.7 cal. ka BP and a shift to a less fresher moisture source and warmer conditions around 14.5 cal. ka BP (Fig. 9). This shift, which is characterized by a $\sim 70\%$ increase in δD_{aq} values, suggests a more meridional flow that routed relatively warmer and moisture-rich air into the region. It is likely that Atteköpsmosse's δD_{aq} record displays a response to the incursion of warm Atlantic waters into the Nordic Seas due to a recovery of the Atlantic Meridional Overturning Circulation after Greenland Stadial 2/Heinrich Stadial 1/Oldest Dryas (Koç Karpuz & Jansen 1992; McManus *et al.* 2004). The change in circulation regime and temperature could therefore have been the underlying trigger for the changes seen around Atteköpsmosse at *c.* 14.7-14.5 cal. ka BP (Fig. 9).

The decrease in δD_{aq} values around 13.7-13.6 cal. ka BP could indicate a shift towards a fresher moisture source and/or colder conditions (Fig. 9). This interpretation is in agreement with more negative δD values of precipitation as also evidenced in the δD_{terr} record (Fig. 8). More negative δD values could indicate higher input of isotopically depleted freshwater at the marine moisture source and/or cooler air temperatures at Atteköpsmosse. However, since the temperature reconstructions derived from chironomid assemblages and plant indicator species do not show any significant summer cooling at this time, we suggest that the negative δD_{aq} shift is mainly associated with an increase in freshwater discharge into the Nordic Seas, likely from the Fennoscandian Ice Sheet.

Between 13.1 and 13.0 cal. ka BP, δD_{aq} values further decrease, indicating a shift towards an even fresher moisture source and/or colder conditions (Fig. 9). A stronger freshening of the marine moisture source and cooling at around this time have also been inferred from Hässeldala Port's hydroclimate records (Muschitiello *et al.* 2015b). Muschitiello *et al.* (2015b) suggested it to be a response to the gradual increase in freshwater discharge into the Nordic Seas, which in turn led to a less efficient moisture production and transport to Northern Europe. The onset of fresher, colder and drier climatic conditions seems to have triggered the series of events seen in Atteköpsmosse's proxy records: lower lake water summer temperatures, frequent forest fires and lower lake aquatic productivity (Fig. 9).

δD_{aq} displays only minor changes at the onset of the Holocene, in contrast to several other proxies (Fig. 9). A similar lack of response is also seen in the δD_{terr} record (Fig. 8). Given that significant changes in vegetation cover only occurred around 11.4 cal. ka BP, we suggest the flat δD signal to be related to a combined effect of a strong freshening of the moisture source in response to

warming and rising air temperatures (Fig. 9). The North Sea /Nordic Seas, which are the main moisture sources for Atteköpsmosse, remained largely fresh after the onset of the Holocene due to enhanced melting of the Fennoscandian Ice Sheet. This in turn would have resulted in a proximal moisture source of precipitation at Atteköpsmosse, which was characterised by very depleted δD waters. We therefore hypothesize that the reason for no appreciable changes in the isotope record is that the isotopic composition of precipitation — and by extension of the marine moisture source — remained substantially unchanged.

Conclusions

With sediments dating back to 15.5 cal. ka BP, Atteköpsmosse is one of the oldest Lateglacial lake records so far reported from northern Europe. The multi-proxy study, combining sediment lithology, geochemistry, biomarkers, hydrogen isotopes, pollen stratigraphy, plant macrofossils, chironomids and a high-resolution chronology, allows for the first time to assess the hydroclimate history, to evaluate the impact of climatic changes on the local environmental, and to discuss the series of events leading into and out of past warm and cold time intervals.

Following the regional deglaciation, stagnant ice remained for about 1500 years and lake infilling did not start until *c.* 15.5 cal. ka BP. The lake and its surroundings were initially characterised by high run-off, low aquatic productivity, cold lake water surface summer temperatures and a scarce herb and shrub vegetation. The inflow of warmer and moisture-rich air masses *c.* 14.7-14.5 cal. ka BP and high minimum mean July air temperatures likely favoured catchment stabilisation, higher aquatic productivity, a rise in lake water surface summer temperatures and the early establishment of tree birch.

Between 14.5 and 13.7 cal. ka BP aquatic productivity gradually increases, chironomid assemblages that are typical for boreal forest lakes appear, diverse herbs, shrubs and dwarf shrubs are present around the ancient lake and reconstructed lake surface water summer temperatures and minimum mean July air temperatures fluctuate around 12-15 °C. A freshening of the moisture source region for Atteköpsmosse is observed around 13.7-13.6 cal. ka BP, likely due to enhanced Fennoscandian Ice Sheet melt. These changes do not seem to have had a large impact on the ancient lake and its catchment, since lake aquatic productivity increased further and lake water summer temperatures and minimum mean July air temperatures remain around 12-14 °C.

Distinct environmental changes took place around and after 13 cal. ka BP, subsequent to a further freshening of the moisture source region. Lake organic productivity starts to decrease, conditions become drier and lake surface water

summer temperatures drop to around 10-12 °C, while minimum July air temperatures remain around 14 °C. Finds of tree *Betula* and *Pinus sylvestris* needles at 13-12.8 cal. ka BP show that these trees were present in the lake's catchment.

The transition into the Holocene is marked by a change in chironomid faunal assemblages, a rise in aquatic productivity and an increase in lake water summer temperatures to 14 °C at 11.6-11.5 cal. ka BP. These changes were followed by the re-establishment of a diverse aquatic and terrestrial vegetation, including tree birch and *Pinus sylvestris* at 11.4 cal. ka BP. Interestingly, the isotope record does not show any changes at this transition, which can be explained by enhanced melting of the Fennoscandian Ice Sheet in response to warming and a proximal moisture source of precipitation at Atteköpsmosse.

Acknowledgements — We would like to thank Margret Steinhorsdottir and Nathalie van der Putten for help during fieldwork, Jayne Rattay, Heike Sigmund and Klara Hajnal for laboratory analyses and Sarah Greenwood for making Figure 1 available. Bodil Liedberg-Jönsson made the first pollen diagram for Atteköpsmosse based on core C-1981. We also thank the two anonymous reviewers, whose comments helped to improve the manuscript. This study was supported by the Swedish Nuclear Fuel and Waste Management Company.

The complete Atteköpsmosse data set will be stored at Bolin Centre Database at <https://bolin.su.se/data/>.

References

- Aichner, B., Herzschuh, U., Wilkes, H., Vieth, A. & Böhner, J. 2010: δD values of n-alkanes in Tibetan lake sediments and aquatic macrophytes - a surface sediment study and application to a 16 ka record from Lake Koucha. *Organic Geochemistry* 41, 779-790.
- Bennike, O., Sarmaja-Korjonen, K. & Seppänen, A. 2004: Reinvestigation of the classic late-glacial Bølling Sø sequence, Denmark: chronology, macrofossils, Cladocera and chydorid ephippia. *Journal of Quaternary Science* 19, 465-478.
- Berglund, B. & Mörner, N.-A. 1984: Late Weichselian deglaciation and chronostratigraphy of southern Scandinavia: problems and present "State of the Art". In Mörner, N.-A. & Karlén, W. (eds.): *Climatic Changes on a Yearly to Millennial Basis*, 17-24. D. Reidel Publishing Company, Dordrecht.

- Berglund, B. E. 1971: Late-glacial stratigraphy and chronology in south Sweden in the light of biostratigraphic studies on Mt. Kullen, Scania. *Geologiska Föreningens i Stockholm Förhandlingar* 93, 11-45.
- Berglund, B. E. 1979: The deglaciation of southern Sweden, 13,500-10,000 BP. *Boreas* 8, 89-118.
- Berglund, B. E., Bergsten, H., Björck, S., Kolstrup, E., Lemdahl, G. & Norberg, K. 1994: Late Weichselian environmental change in southern Sweden and Denmark. *Journal of Quaternary Science* 9, 127-132.
- Berglund, B. E. & Malmer, N. 1971: Soil conditions and Late-glacial stratigraphy. *Geologiska Föreningen i Stockholm Förhandlingar* 93, 575-586.
- Berglund, B. E. & Ralska-Jasiewiczowa, M. 1986: Pollen analysis and pollen diagrams. In Berglund, B. E. (ed.): *Handbook of Holocene Palaeoecology and Palaeohydrology*, 455-484. John Wiley & Sons, Chichester.
- Björck, S. 1981: A stratigraphic study of Late Weichselian deglaciation, shore displacement and vegetation history in south-eastern Sweden. *Fossils and Strata* 14, 1-93.
- Björck, S., Kromer, B., Johnsen, S., Bennike, O., Hammarlund, D., Lemdahl, G., Possnert, G., Rasmussen, T. L., Wohlfarth, B., Hammer, C. U. & Spurk, M. 1996: Synchronised terrestrial-atmospheric deglacial records around the North Atlantic. *Science* 274, 1155-1160.
- Björck, S. & Möller, P. 1987: Late Weichselian environmental history in southeastern Sweden during the deglaciation of the Scandinavian ice sheet. *Quaternary Research* 28, 1-37.
- Blockley, S. P. E., Ramsey, C. B., Lane, C. S. & Lotter, A. F. 2008: Improved age modelling approaches as exemplified by the revised chronology for the Central European varved lake Soppensee. *Quaternary Science Reviews* 27, 61-71.
- Bronk Ramsey, C. 2008: Deposition models for chronological records. *Quaternary Science Reviews* 27, 42-60.
- Bronk Ramsey, C. 2009: Bayesian analysis of radiocarbon dates. *Radiocarbon* 51, 337-360.
- Bronk Ramsey, C. 2010: *OxCal Program, v.4.1.7*. Radiocarbon Accelerator Unit, University of Oxford, UK.
- Brooks, S. J., Langdon, P. G. & Heiri, O. 2007: The identification of Paleoarctic Chironomidae larvae in palaeoecology. *QRA Technical Guide* 10, 1-276.
- Bush, R. T. & McInerney, F. A. 2013: Leaf wax n-alkane distributions in and across modern plants: implications for paleoecology and chemotaxonomy. *Geochimica et Cosmochimica Acta* 117, 161-179.
- Comas-Cufí, M. & Thió-Henestrosa, S. 2011: *CoDaPack 2.0. 2.0 ed.* Universitat de Girona, Spain.
- Davies, S. M., Turney, C. S. M. & Lowe, J. J. 2001: Identification and significance of a visible, basalt-rich Vedde Ash layer in a Late-glacial sequence on the Isle of Skye, Inner Hebrides, Scotland. *Journal of Quaternary Science* 16, 99-104.
- Davies, S. M., Wastegård, S. & Wohlfarth, B. 2003: Extending the limits of the Borrobol Tephra to Scandinavia and detection of new early Holocene tephra. *Quaternary Research* 59, 345-352.

- Diefendorf, A. F., Freeman, K. H., Wing, S. L. & Graham, H. V. 2011: Production of n-alkyl lipids in living plants and implications for the geologic past. *Geochimica et Cosmochimica Acta* 75, 7472–7485.
- Eglinton, G. & Hamilton, R. G. 1967: Leaf epicuticular waxes. *Science* 156, 1322-1335.
- Ficken, K. J., Li, B., Swain, D. L. & Eglinton, G. 2000: An n-alkane proxy for the sedimentary input of submerged/floating freshwater aquatic macrophytes. *Organic Geochemistry* 31, 745-749.
- Fischer, A., Mortensen, M. F., Henriksen, P. S., Mathiassen, D. R. & Olsen, J. 2013: Dating the Trollesgave site and the Bromme culture – chronological fix-points for the Lateglacial settlement of Southern Scandinavia. *Journal of Archaeological Science* 40, 4663-4674.
- Gao, L., Hou, J., Toney, J., MacDonald, D. & Huang, Y. 2011: Mathematical modeling of the aquatic macrophyte inputs of mid-chain n-alkyl lipids to lake sediments: implications for interpreting compound specific hydrogen isotopic records. *Geochimica et Cosmochimica Acta* 75, 3781-3791.
- Gibson, J. J. 2002: Short-term evaporation and water budget comparisons in shallow Arctic lakes using non-steady isotope mass balance. *Journal of Hydrology* 264, 242-261.
- Gustafsson, M., Rayner, D. & Chen, D. 2010: Extreme rainfall events in southern Sweden: Where does the moisture come from? *Tellus Series A* 62, 605-616.
- Håkansson, S. 1984: University of Lund Radiocarbon Dates XVII. *Radiocarbon* 26, 392-411.
- Hammarlund, D. 1999: Ostracod stable isotope records from a deglacial isolation sequence in southern Sweden. *Boreas* 28, 564-574.
- Hammarlund, D. & Lemdahl, G. 1994: A late Weichselian stable isotope stratigraphy compared with biostratigraphical data: a case study from southern Sweden. *Journal of Quaternary Science* 9, 13-31.
- Hayward, C. 2012: High spatial resolution electron probe microanalysis of tephra and melt inclusions without beam-induced chemical modification. *The Holocene* 22, 119-125.
- Heiri, O. & Lotter, A. F. 2001: Effect of low count sums on quantitative environmental reconstructions: an example using subfossil chironomids. *Journal of Paleolimnology* 23, 343-350.
- Housley, R. A., MacLeod, A., Nalepka, D., Jurochnik, A., Masojc, M., Davies, L., Lincoln, P., Bronk Ramsey, C., Gamble, C. & Lowe, J. J. 2013: Tephrostratigraphy of a Lateglacial lake sediment sequence at Wegliny, southwest Poland. *Quaternary Science Reviews* 77, 4-18.
- Hughes, A. L. C., Gyllencreutz, R., Lohne, S. O., Mangerud, J. & Svendsen, J. I. 2016: The last Eurasian ice sheets – a chronological database and time-slice reconstruction, DATED-1. *Boreas* 45, 1-45.
- Juggins, S. 2007: *C2 Version 1.5 User guide. Software for ecological and palaeoecological data analysis and visualisation. 1.5 ed.* University of Newcastle, Newcastle upon Tyne, UK.
- Koç Karpuz, N. & Jansen, E. 1992: A high-resolution diatom record of the last deglaciation from the SE Norwegian Sea: documentation of rapid climate changes. *Paleoceanography* 7, 499-520.

- Kylander, M. E., Klaminder, J., Wohlfarth, B. & Löwemark, L. 2013: Geochemical responses to paleoclimatic changes in southern Sweden since the late glacial: the Hässeldala Port lake sediment record. *Journal of Paleolimnology* 50, 57-70.
- Lagerlund, E. 1977: Till studies and neotectonic s in northwest Scania, South Sweden. *Boreas* 6, 159-166.
- Lagerlund, E., Knutsson, G., Åmark, M., Hebrand, M., Jönsson, L.-O., Karlgren, B., Kristiansson, J., Möller, P., Robison, J. M., Sandgren, P., Terne, T. & Waldemarsson, D. 1983: The deglaciation pattern and dynamics in south Sweden, a preliminary report. *LUNDQUA Report 24*, 1-24.
- Lampinen, R., Lahti, T. & Heikkinen, M. 2014: Kasviatlas 2013. Helsingin Yliopisto, Luonnontieteellinen keskusmuseo, Helsinki, Finland. <http://www.luomus.fi/kasviatlas>.
- Lane, C. S., Blockley, S. P. E., Bronk Ramsey, C. & Lotter, A. F. 2011: Tephrochronology and absolute centennial scale synchronisation of European and Greenland records for the last glacial to interglacial transition: A case study of Soppensee and NGRIP. *Quaternary International* 246, 145-156.
- Lane, C. S., De Klerk, P. & Cullen, V. L. 2012a: A tephrochronology for the Lateglacial palynological record of the Endinger Bruch (Vorpommern, north-east Germany). *Journal of Quaternary Science* 27, 141-149.
- Lane, C. S., Blockley, S. P. E., Mangerud, J., Smith, V. C., Lohne, O. S., Tomlinson, E. L., Matthews, I. P. & Lotter, A. F. 2012b: Was the 12.1 ka Icelandic Vedde Ash one of a kind? *Quaternary Science Reviews* 33, 87-99.
- Lane, C. S., Blockley, S. P. E., Mangerud, J., Smith, V. C., Lohne, O. S., Tomlinson, E. L., Matthews, I. P. & Lotter, A. F. 2012c: Was the 12.1 ka Icelandic Vedde Ash one of a kind? *Quaternary Science Reviews* 33, 87-99.
- Lane, C. S., Blockley, S. P. E., Lotter, A. F., Finsinger, W., Filippi, M. L. & Matthews, I. P. 2012d: A regional tephrostratigraphic framework for central and southern European climate archives during the Last Glacial to Interglacial transition: comparisons north and south of the Alps. *Quaternary Science Reviews* 36, 50-58.
- Larsen, J. J. & Noe-Nygaard, N. 2014: Lateglacial and early Holocene tephrostratigraphy and sedimentology of the Store Slotseng basin, SW Denmark: a multi-proxy study. *Boreas* 43, 349-361.
- Lemdahl, G. 1988: Palaeoclimatic and palaeoecological studies based on subfossil insects from Late Weichselian sediments in southern Sweden. *LUNDQUA Thesis* 22, 1-11.
- Liedberg-Jönsson, B. 1988: The Late Weichselian macrofossil flora in western Skåne, southern Sweden. *LUNDQUA Thesis* 24, 1-82.
- Lind, E. M. & Wastegard, S. 2011: Tephra horizons contemporary with short early Holocene climate fluctuations: New results from the Faroe Islands. *Quaternary International* 246, 157-161.
- Lind, E. M., Wastegard, S. & Larsen, J. J. 2013: A Late Younger Dryas-Early Holocene tephrostratigraphy for Fosen, Central Norway. *Journal of Quaternary Science* 28, 803-811.
- Lundqvist, J. & Wohlfarth, B. 2001: Timing and east-west correlation of south Swedish ice marginal lines during the Late Weichselian. *Quaternary Science Reviews* 20, 1127-1148.

- Luoto, T. P. & Nevalainen, L. 2013: Long-term water temperature reconstructions from mountain lakes with different catchment and morphometric features. *Scientific Reports* 3, 2488. DOI:10.1038/srep02488.
- Luoto, T. P., Rantala, M. V., Galkin, A., Rautio, M. & Nevalainen, L. 2016: Environmental determinants of chironomid communities in remote northern lakes across the treeline - Implications for climate change assessments. *Ecological Indicators* 61, 991-999.
- Matthews, I. P., Birks, H. H., Bourne, A. J., Brooks, S. J., Lowe, J. J., Macleod, A. & Pyne-O'Donnell, S. D. F. 2011: New age estimates and climatostratigraphic correlations for the Borrobol and Penifiler Tephra: evidence from Abernethy Forest, Scotland. *Journal of Quaternary Science* 26, 247-252.
- McManus, J. F., Francois, R., Gherardi, J. M., Keigwin, L. D. & Brown-Leger, S. 2004: Collapse and rapid resumption of Atlantic meridional circulation linked to deglacial climate changes. *Nature* 428, 834-837.
- Mortenson, M. F., Birks, H. H., Christensen, C., Holm, J., Noe-Nygaard, N., Odgaard, B. V., Olsen, J. & Rasmussen, K. L. 2011: Lateglacial vegetation development in Denmark – New evidence based on macrofossils and pollen from Slotseng, a small-scale site in southern Jutland. *Quaternary Science Reviews* 30, 2534-2550.
- Mortenson, M. F., Henriksen, P. S., Christensen, C., Petersen, P. V. & Olsen, J. 2014: Vegetation development in south-east Denmark during the Weichselian Late Glacial: palaeoenvironmental studies close to the Palaeolithic site of Hasselø. *Danish Journal of Archaeology* 3, 33-51. DOI: 10.1080/21662282.2014.994281
- Muscheler, R., Adolphi, F. & Knudsen, M.F. 2014: Assessing the differences between the IntCal and Greenland ice-core time scales for the last 14,000 years via the common cosmogenic radionuclide variations. *Quaternary Science Reviews* 106, 81–87.
- Muschitiello, F., Andersson, A., Wohlfarth, B. & Smittenberg, R. H. 2015a: The C₂₀ highly branched isoprenoid biomarker – A new diatom-sourced proxy for summer trophic conditions? *Organic Geochemistry* 81, 27-33.
- Muschitiello, F., Pausata, F. S. R., Smittenberg, R. H., Salih, A. A. M., Watson, J. E., Brooks, S. J., Whitehouse, N. J., Karlatou-Charalampopoulou, A. & Wohlfarth, B. 2015b: Fennoscandian freshwater control on Greenland hydrological shifts at the onset of the Younger Dryas. *Nature Communications* 6, DOI: 10.1038/ncomms9939.
- Muschitiello, F., Lea, J., Greenwood, S. L., Nick, F. M., Brunnberg, L., MacLeod, A. & Wohlfarth, B. 2016: Precise timing of the first drainage of the Baltic Ice Lake from Swedish glacial-varve chronologies. *Boreas* 45, 322-334.
- Nesbitt, H. W. & Markovics, G. 1997: Weathering of granodioritic crust, long-term storage of elements in weathering profiles, and petrogenesis of siliciclastic sediments. *Geochimica et Cosmochimica Acta* 61, 1653-1670.
- Ott, F., Wulf, S., Serb, J., Slowinski, M., Obremaska, M., Tjallingii, R., Blaszkiewicz, M. & Brauer, A. 2016: Constraining the time span between Early Holocene Håsseldalen and Aska-S Tephra through varve counting in the Lake Czechowskie sediment record, Poland. *Journal of Quaternary Science* 31, 103-113.

- Pyne-O'Donnell, S. D. F. 2007: Three new distal tephras in sediments spanning the Last Glacial-Interglacial Transition in Scotland. *Journal of Quaternary Science* 22, 559-570.
- Rach, O., Brauer, a., Wilkes, H. & Sachse, D. 2014: Delayed hydrological response to Greenland cooling at the onset of the Younger Dryas in western Europe. *Nature Geoscience* 7, 109-112.
- Ranner, P. H., Allen, J. R. M. & Huntley, B. 2005: A new early Holocene cryptotephra from northwest Scotland. *Journal of Quaternary Science* 20, 201-208.
- Rasmussen, S. O., Andersen, K. K., Svensson, A. M., Steffensen, J. P., Vinther, B. M., Clausen, H. B., Siggaard-Andersen, M. L., Johnsen, S. J., Larsen, L. B., Dahl-Jensen, D., Bigler, M., Röthlisberger, R., Fischer, H., Goto-Azuma, K., Hansson, M. E. & Ruth, U. 2006: A new Greenland ice core chronology for the last glacial termination. *Journal of Geophysical Research* 111, D6. DOI: 10.1029/2005JD006079.
- Rasmussen, S. O., Bigler, M., Blockley, S. P. E., Blunier, T., Buchardt, S. L., Clausen, H. B., Cvijanovic, I., Dahl-Jensen, D., Johnsen, S. J., Fischer, H., Gkinis, V., Guillevic, M., Hoek, W. Z., Lowe, J. J., Pedro, J., Popp, T., Seierstad, I. K., Steffensen, J. P., Svensson, A. M., Vallelonga, P., Vinther, B. M., Walker, M. J. C., Wheatley, J. J. & Winstrup, M. 2014: Stratigraphic framework for robust naming and correlation of abrupt climatic changes during the last glacial period based on three synchronized Greenland ice core records. *Quaternary Science Reviews* 106, 14-28.
- Reimer, P. J., Bard, E., Bayliss, A., Warren Beck, J. W., Blackwell, P. G., Bronk Ramsey, C., Buck, C. E., Cheng, H., Lawrence Edwards, R. L., Friedrich, M., Grootes, P. M., Hafliðason, H., Hajdas, I., Hatté, C., Heaton, T. J., Hoffmann, D. L., Hogg, A. G., Hughen, K. A., Kaiser, K. F., Kromer, B., Manning, S. W., Niu, M., Reimer, R. W., Richards, D. A., Scott, E. M., Southon, J. R., Staff, R. A., Turney, C. S. M. & van der Plicht, J. 2013: INTCAL13 and MARINE13 Radiocarbon age calibration curves 0–50,000 years cal BP. *Radiocarbon* 55, 1869–1887.
- Sachse, D., Billault, I., Bowen, G. J., Chikaraishi, Y., Dawson, T. E., Feakins, S. J., Freeman, K. H., Magill, C. R., McInerney, F., van der Meer, M. T. J., Polissar, P., Robins, R. J., Sachs, J. P., Schmidt, H.-L., Sessions, A. L., White, J. W. C., West, J. B. & Kahmen, A. 2012: Molecular paleohydrology: Interpreting the hydrogen-isotopic composition of lipid biomarkers from photosynthesizing organisms. *Annual Review of Earth and Planetary Sciences* 40, 221-249.
- Sachse, D., Radke, J. & Gleixner, G. 2004: Hydrogen isotope ratios of recent lacustrine sedimentary n-alkanes record modern climate variability. *Geochimica et Cosmochimica Acta* 68, 4877–4889.
- Sandgren, P. 1983: The deglaciation of the Klippan area, southern Sweden – a study of glaciofluvial and glaciomarine sediments. *LUNDQUA Thesis* 14, 1-99.
- Sandgren, P. & Snowball, I. 2001: The Late Weichselian sea level history of the Kullen Peninsula in northwest Skåne, southern Sweden. *Boreas* 30, 115-130.
- Sandgren, P., Snowball, I. F., Hammarlund, D. & Risberg, J. 1999: Stratigraphic evidence for a high marine shore-line during the Late Weichselian

deglaciation on the Kullen Peninsula, southern Sweden. *Journal of Quaternary Science* 14, 223-237.

SMHI (2017): Normal årsmedeltemperatur och års medelnederbörd (1961-1990).

www.smhi.se/klimatdata/meteorologi/kartor/monYrTable.php?myn=12&par=normYrTmp;

(<https://www.smhi.se/klimatdata/meteorologi/nederbord/normal-uppmatt-arsnederbord-medelvarde-1961-1990-1.4160>).

Steinhorsdottir, M., Wohlfarth, B., Kylander, M., Blaauw, M. & Reimer, P. J. 2013: Stomatal proxy record of CO₂ concentrations from the last termination suggests an important role for CO₂ at climate change transitions. *Quaternary Science Reviews* 68, 43-58.

Steffensen, J. P., Andersen, K. A., Bigler, M., Clausen, H. B., Dahl-Jensen, D., Fischer, H., Goto-Azuma, K., Hansson, M., Johnsen, S. J., Jouzel, J., Masson-Delmotte, V., Popp, T., Rasmussen, S. O., Röthlisberger, R., Ruth, U., Stauffer, B., Siggaard-Andersen, M. L., Sveinbjörnsdóttir, A. E., Svensson, A. and White, J. W. C. 2008: High-resolution Greenland ice core data show abrupt climate change happens in few years. *Science* 321, 680-684.

Stroeven, A., Hättestrand, C., Kleman, J., Heyman, J., Fabel, D., Fredin, O., Goodfellow, B. W., Harbor, J. M., Jansen, J. D., Olsen, L., Caffee, M. W., Fink, D., Lundqvist, J., Risqvist, G. C., Strömberg, B. & Jansson, K. N. 2016: Deglaciation of Fennoscandia. *Quaternary Science Reviews* 147, 91-121.

Terberger, T., De Klerk, P., Helbig, H., Kaiser, K. & Kühn, P. 2004: Late Weichselian landscape development and human settlement in Mecklenburg-Vorpommern (NE Germany). *Eiszeitalter und Gegenwart* 54, 138-175.

Turney, C. S. M. 1998: Extraction of rhyolitic component of Vedde microtephra horizons to correlate lake sediments. *Journal of Paleolimnology* 19, 199-206.

Väliranta, M., Salonen, J. S., Heikkilä, M., Amon, L., Helmens, K. F., Klimaschewski, A., Kuhry, P., Kultti, S., Poska, A., Shala, S., Veski, S. & Birks, H. H. 2015: Plant macrofossil evidence for an early onset of the Holocene summer thermal maximum in northern Europe. *Nature Communications* 6, 6809. DOI: 10.1038/ncomms7809.

Venäläinen, A., Tuomenvirta, H., Pirinen, P. & Drebs, A. A. 2005: Basic climate data set 1961-2000 - descriptions and illustrations *Finnish Meteorological Institute Report 2005-5*, 1-27.

Veres, D. 2001: *A comparative study between loss on ignition and total carbon analysis on Late Glacial sediments from Atteköps mosse, southwestern Sweden, and their tentative correlation with the GRIP event stratigraphy*. M.Sc. thesis 145, 36 pp. Department of Geology, Lund University.

Walker, M. & Lowe, J. 2017: Lateglacial environmental change in Scotland. *Earth and Environmental Science Transactions of the Royal Society of Edinburgh*. <https://doi.org/10.1017/S1755691017000184>.

Watson, J. 2008: *Quantifying Late Glacial climate change in Northwestern Europe using two insect proxies*. Ph.D. thesis, The Queen's University of Belfast, 365 pp.

- Weltje, G. J., Bloemsma, M. R., Tjallingii, R., Heslop, D., Röhl, U. & Croudace, I. W. 2015: Prediction of geochemical composition from XRF core scanner data: A new multivariate approach including automatic selection of calibration samples and quantification of uncertainties. *In* Croudace, I. W. & Rothwell, R. G. (eds.): *Micro-XRF Studies of Sediment Cores: Applications of a non-destructive tool for the environmental sciences*, 507-534. Springer, Dordrecht.
- Weltje, G. J. & Tjallingii, R. 2008: Calibration of XRF core scanners for quantitative geochemical logging of sediment cores: Theory and application. *Earth and Planetary Science Letters* 274, 423-438.
- Wetzel, R. G. 2001: *Limnology*. 1006 pp. Academic Press, San Diego.
- Wohlfarth, B., Muschitiello, F., Greenwood, S. L., Andersson, A., Kylander, M., Smittenberg, R. H., Steinthorsdottir, M., Watson, J. & Whitehouse, N. J. 2017: Hässeldala – a key site for Last Termination climate events in northern Europe. *Boreas* 46, 143-161.
- Wulf, S., Dräger, N., Ott, F., Serb, J., Appelt, O., Guðmundsdóttir, E., van den Bogaard, C., Slowinski, M., Blaszkiewicz, M. & Brauer, A. 2016a: Holocene tephrostratigraphy of varved sediment records from Lakes Tiefer See (NE Germany) and Czechowskie (N Poland). *Quaternary Science Reviews* 132, 1-14.

Figures and Tables

Figure 1. A-B. Location of the study area in southwest Sweden (inset figure) and topography and position of the Fennoscandian Ice Sheet margin and of the marine limit ~17 and ~15 cal. ka BP, respectively. The maximum (white dashed line), mean (white transparent) and minimum (black dashed line) positions of the Fennoscandian Ice Sheet margin at ~17 and ~15 cal. ka BP follow Hughes *et al.* (2016). The marine limit (thin blue line) has been estimated to 88 m a.s.l. (~17 cal. ka BP) and to 77 m a.s.l. (~15 cal. ka BP) based on studies on Kullen Peninsula (Sandgren & Snowball 2001). The location of Atteköpsmosse on Hallandsåsen is shown by a filled white square. Atteköpsmosse receives most of its precipitation from the North Sea and the Nordic Seas. Important sites on Kullen Peninsula (Björkerödsmosse, Håkullsmosse) (Berglund & Ralska-Jasiewiczowa 1986; Liedberg-Jönsson 1988) are marked by a filled black square. C. Close-up of the topography around Atteköpsmosse (marked in red). This part of Hallandsåsen contains numerous peatbogs (light brown with black dashed lines) and few lakes, but early lateglacial sediments have only been found in Atteköpsmosse (Björck & Liedberg-Jönsson, unpublished).

Figure 2. A. Lithostratigraphy and loss-on-ignition (LOI) curve for Atteköpsmosse core C-2011. Details on the tephra found at 508-509 cm depth

(ATK 508-509) can be found in Fig. 3, in the text and in Table S2. B. Lithostratigraphy and loss-on-ignition (LOI) curve for Atteköpsmosse core C-1981 (Björck and Liedberg-Jönsson, unpublished). A lithostratigraphic description for both cores is given in Table S1.

Figure 3. Major element bi-plots showing single-grain analyses for the tephra found at 508-509 cm depth (ATK 508-509) in Atteköpsmosse core C-2011. Data are normalized to an anhydrous basis. Also shown are the composition of other tephtras of Younger Dryas and early Holocene age identified in Northwestern Europe: Hässeldalen (Davies *et al.* 2003; Lind & Wastegard 2011; Lane *et al.* 2012a; Wulf *et al.* 2016), Vedde Ash (Davies *et al.* 2001, 2003; Lind & Wastegard 2011; Lane *et al.* 2011, 2012b, c, d), Ashik (Pyne-O'Donnell 2007), Fosen (Lind *et al.* 2013), Breakish (Pyne-O'Donnell 2007), An Druim (Ranner *et al.* 2005) and AF555 (Matthews *et al.* 2011). Single-grain analyses for ATK 508-509 are given in Table S2.

Figure 4. A. Age-depth model for Atteköpsmosse core C-2011 based on the Bayesian analysis procedure of OxCal4.2. The dark and light green envelopes show the modelled 68% and 95% calendar age confidence intervals, respectively. The light grey distribution curves indicate the 95% confidence interval for each calibrated ^{14}C date and the dark grey distribution curves and the bold black lines are the respective 68% confidence intervals. B. Monte Carlo-based stratigraphic alignment of Atteköpsmosse cores C-1981 (red line) and C-2011 (black line) using their respective loss-on-ignition (LOI) curves. See text for further explanations and Table 1 for the complete list of ^{14}C dates used to build the age model.

Figure 5. Percentage diagram for selected pollen taxa for Atteköpsmosse core C-1981 (Björck and Liedberg-Jönsson, unpublished). Smaller *Betula nana* -type pollen and larger *Betula pubescens* - type pollen were differentiated based on pollen size. Local pollen assemblage zones were established visually and identified based on pollen frequencies and are correlated to the regional pollen zones of Liedberg-Jönsson (1988). Single occurrences of specific pollen taxa are shown (T = *Typha latifolia*; M = *Myriophyllum spicatum*). The thin-lined percentage curves represent a 10 x exaggeration. See Fig. 2 for a lithostratigraphic legend.

Figure 6. Selected plant macrofossil taxa for Atteköpsmosse core C-2011 and visually established plant macrofossil zones. The most abundant bryophyte taxa were grouped together and are dominated by *Scorpidium scorpioides* and *Warnstofia exannulata* - group; other species were only detected as scattered

individual leaf remains (*Aulacomnium palustre*, *Calliergon* sp., *Cinclidium stygium*, *Climacium dendroides*, *Paludella squarrosa*, *Polytrichum* sp., *Polytrichum jensenii*, *Polytrichum strictum*, *Rhizomnium* s.l., *Sphagnum squarrosum*, *Straminergon stramineum* and *Tomemtypnum nitens*). The horizontal black bars show the exact number of finds in each sample and black dots the relative abundance of remains (one dot = rare; two dots = occasional; three dots = abundant). No samples were available between 542 and 518 cm depth. O = oospores; S = seeds; Lt = leaf tips; L = leaf, leaf remains; V = vegetative remains; B = bark; C = catkin scale; N = needle, b = bud scales; Sc = fungi sclerotia. See Fig. 2 for a lithostratigraphic legend.

Figure 7. Chironomid percentage diagram for Atteköpsmosse core C-2011. The chironomid zones were established using cluster analysis. De-trended correspondence analysis (DCA) was used to detect variance in chironomid assemblages. DCA was run with square-root species transformation and down-weighting of rare species. See Fig. 2 for a lithostratigraphic legend.

Figure 8. Lithostratigraphy, organic carbon, major elements, bulk geochemistry, biomarkers and hydrogen isotopes for Atteköpsmosse core C-2011. K is used here as a representative for the silica-hosted elements Si, Ti and Rb (see Fig. S1 for more information) and is expressed as centred-log ratio (clr). δD *n*-C₂₃ and δD of C₂₀ HBI represent aquatic biomarkers (δD_{aq}), while δD *n*-C₂₉ represents terrestrial biomarkers (δD_{terr}) (see also Fig. S2). The lithostratigraphic legend is shown in Fig. 2.

Figure 9. Palaeoenvironmental summary for Atteköpsmosse using the combined data set of cores C-2011 and C-1981. A legend to the lithostratigraphy is shown in Fig. 2. The pollen stratigraphy is based on C-1981, while all other proxies (LOI, chironomids, plant macrofossils, geochemistry) have been established on C-2011. Minimum summer temperature estimates are based on plant indicator species of Atteköpsmosse (black dashed line) and Björkeröds- and Håkullsmosse (grey dashed line) (Liedberg-Jönsson 1988) (see also Tables 2 and 3). M = plant macrofossil based minimum summer temperature estimates; P = pollen based minimum summer temperature estimates. The Greenland event stratigraphy follows Rasmussen *et al.* (2014) and Muscheler *et al.* (2014).

Table 1: Radiocarbon dates for Atteköpsmosse cores C-1981 (Håkansson 1984) and C-2011 (this study). The ^{14}C dates of C-2011 were used to construct the age model shown in Fig. 4. See text for further details. Numbers in brackets display the number of plant remains, which were included in each radiocarbon-dated sample. L = leaf, leaf fragments; T = twig; B = buds; F = flower; C = catkin; S = seed, Cc = charcoal, Bk = bark. C-1981 was recovered and sampled in 1981 and C-2011 was cored in autumn 2011 and sub-sampled in autumn 2014.

Table 2: Minimum mean July temperature requirements for terrestrial and aquatic/telmatic indicator plant species found in the Lateglacial/early Holocene sediments of Atteköpsmosse (this study), Björkerödsmosse and Håkullsmosse (Liedberg-Jönsson 1988) (Fig. 1A) according to the methodological approach presented in Välranta *et al.* (2015). Species-specific limiting temperatures were estimated as the median of the mean July temperature values in grid cells containing individual species occurrences along the northernmost modern distribution limit in Finland.

Table 3: Terrestrial and limnic/telmatic plant macrofossil remains in the Lateglacial sediments of Björkerödsmosse (cores BP1, A6) and Håkullsmosse (cores X4, B8:6) on Kullen Peninsula (Liedberg-Jönsson 1988) (Fig. 1A). The Younger Dryas/Preboreal transition as shown in Liedberg-Jönsson (1988) was adapted to the new chronology of Björck *et al.* (1996). Minimum mean July temperatures are according to Välranta *et al.* (2015); see text and Table 2 for more details.

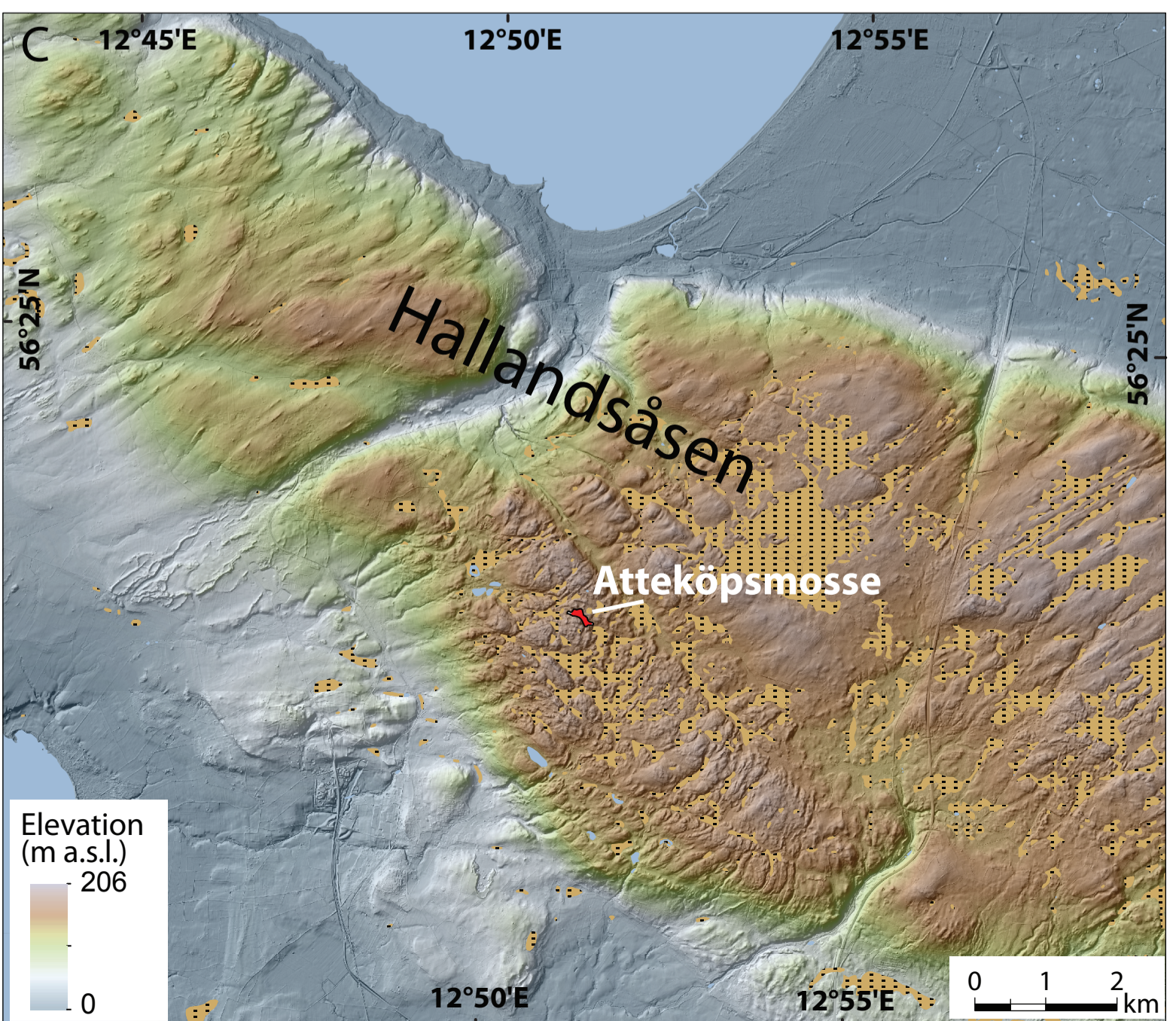
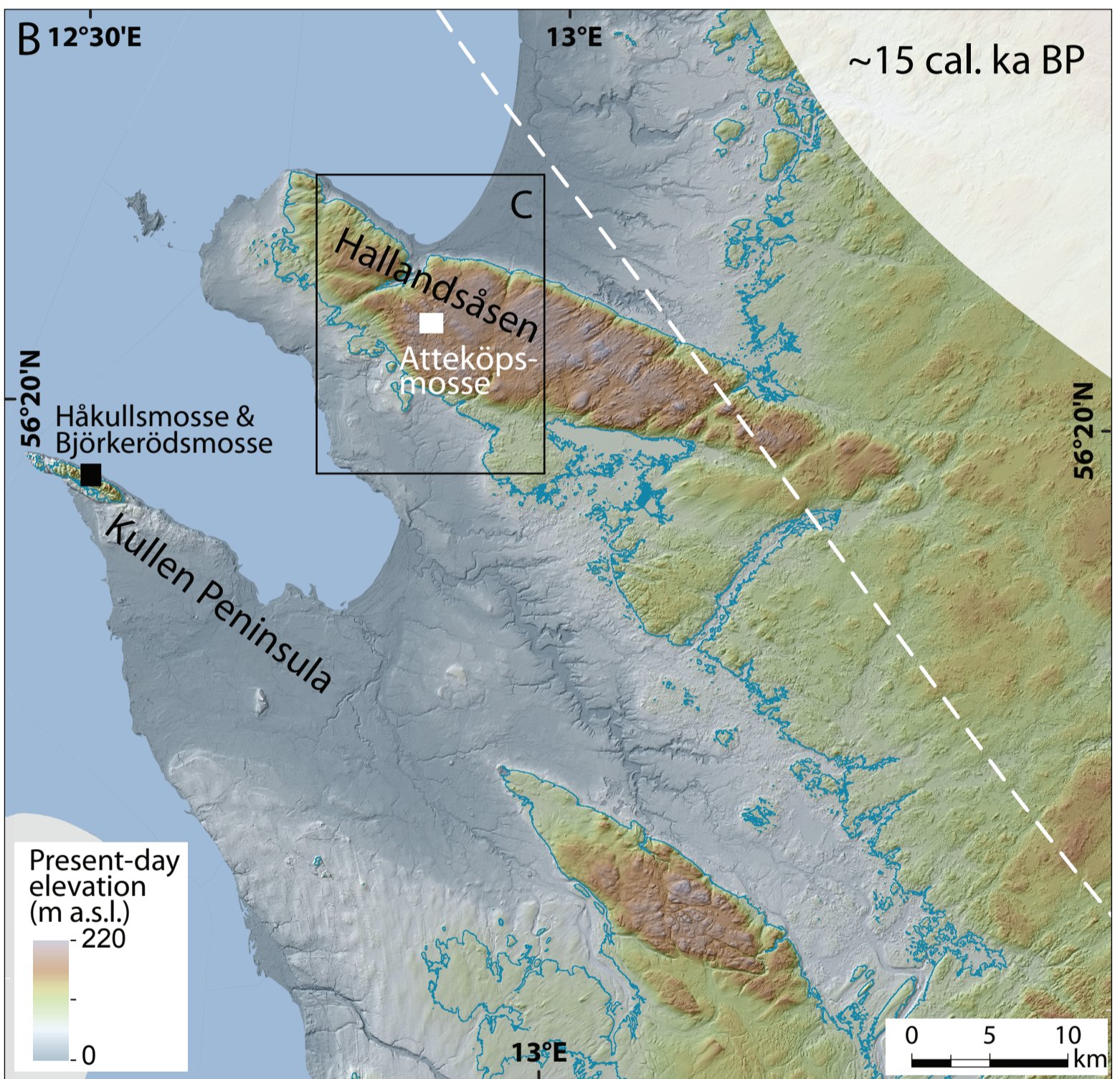
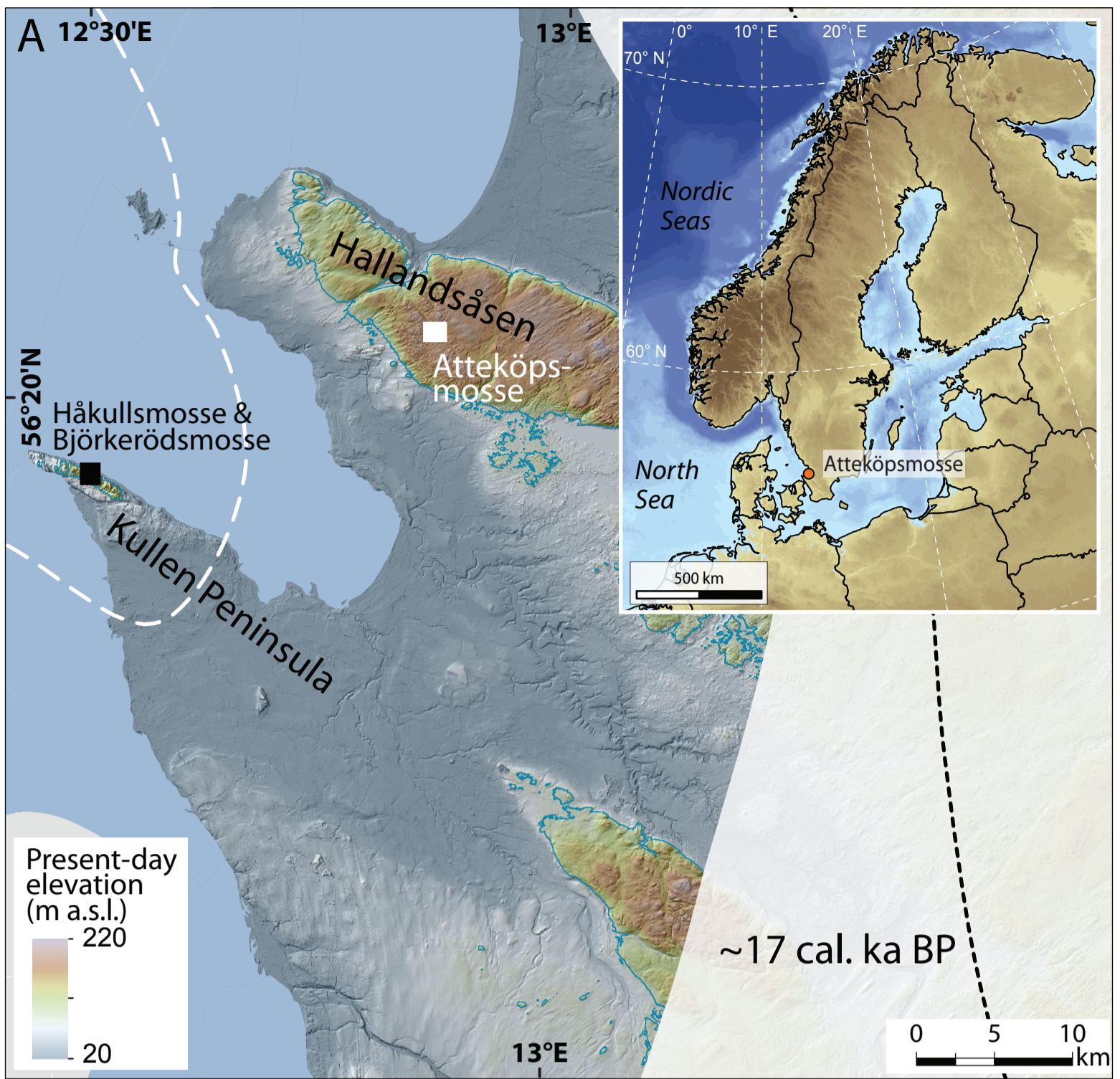
Supporting Information

Fig. S1: Extended XRF data set for Atteköpsmosse core C-2011.

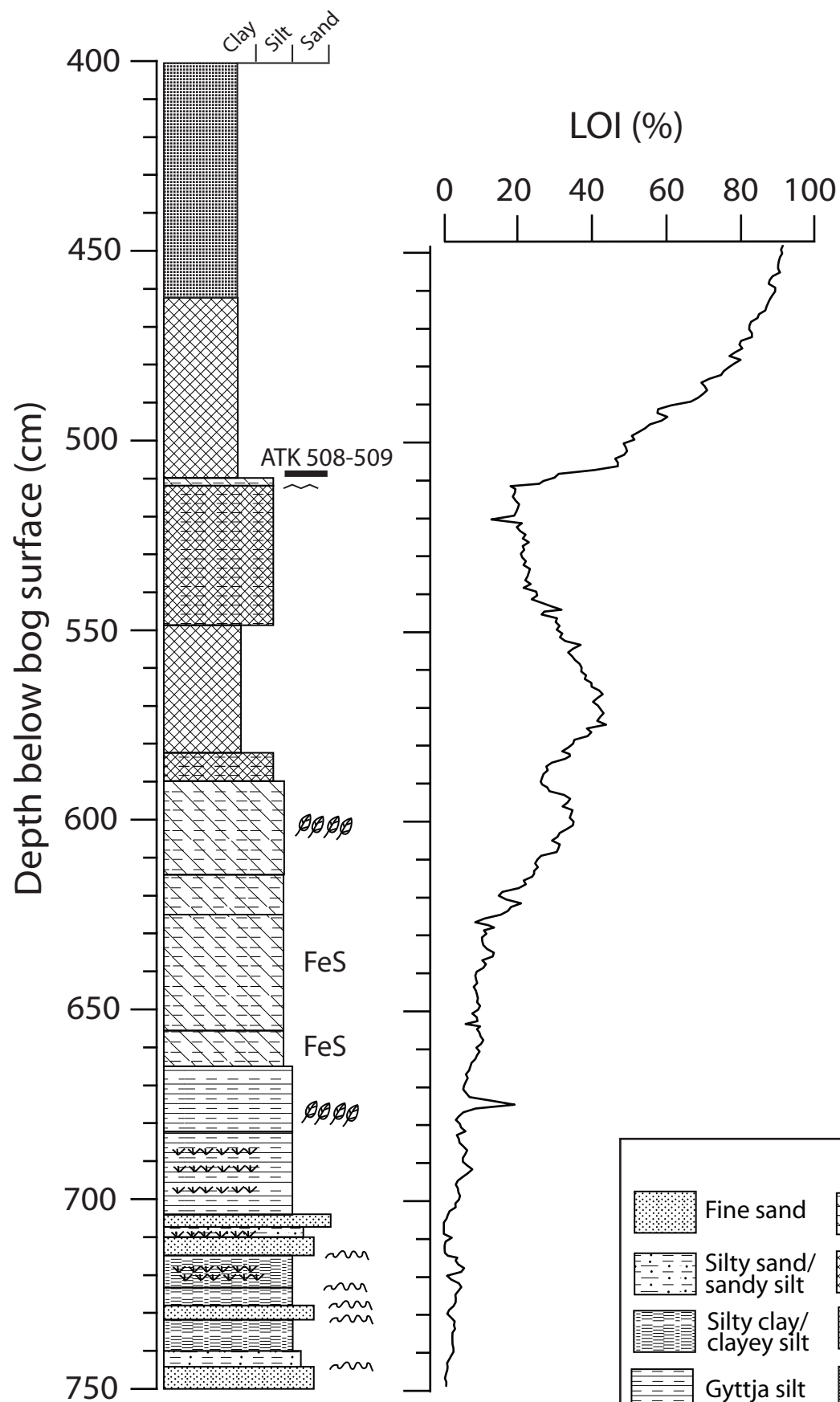
Fig. S2: Scatterplot of the $\delta\text{D } n\text{-C}_{23}$ ($\delta\text{D}_{\text{aq}}$) and $\delta\text{D } n\text{-C}_{29}$ ($\delta\text{D}_{\text{terr}}$) data sets for core C-2011.

Table S1: Lithostratigraphy of the Atteköpsmosse sediment profiles. Composite stratigraphy (A) of core C-2011 and (B) of core C-1981. s = sharp; vs = very sharp; g = gradual; vg = very gradual; LB = lower boundary.

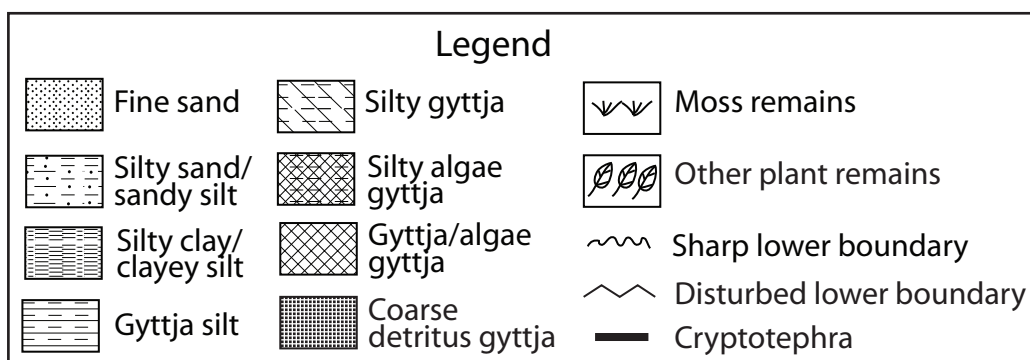
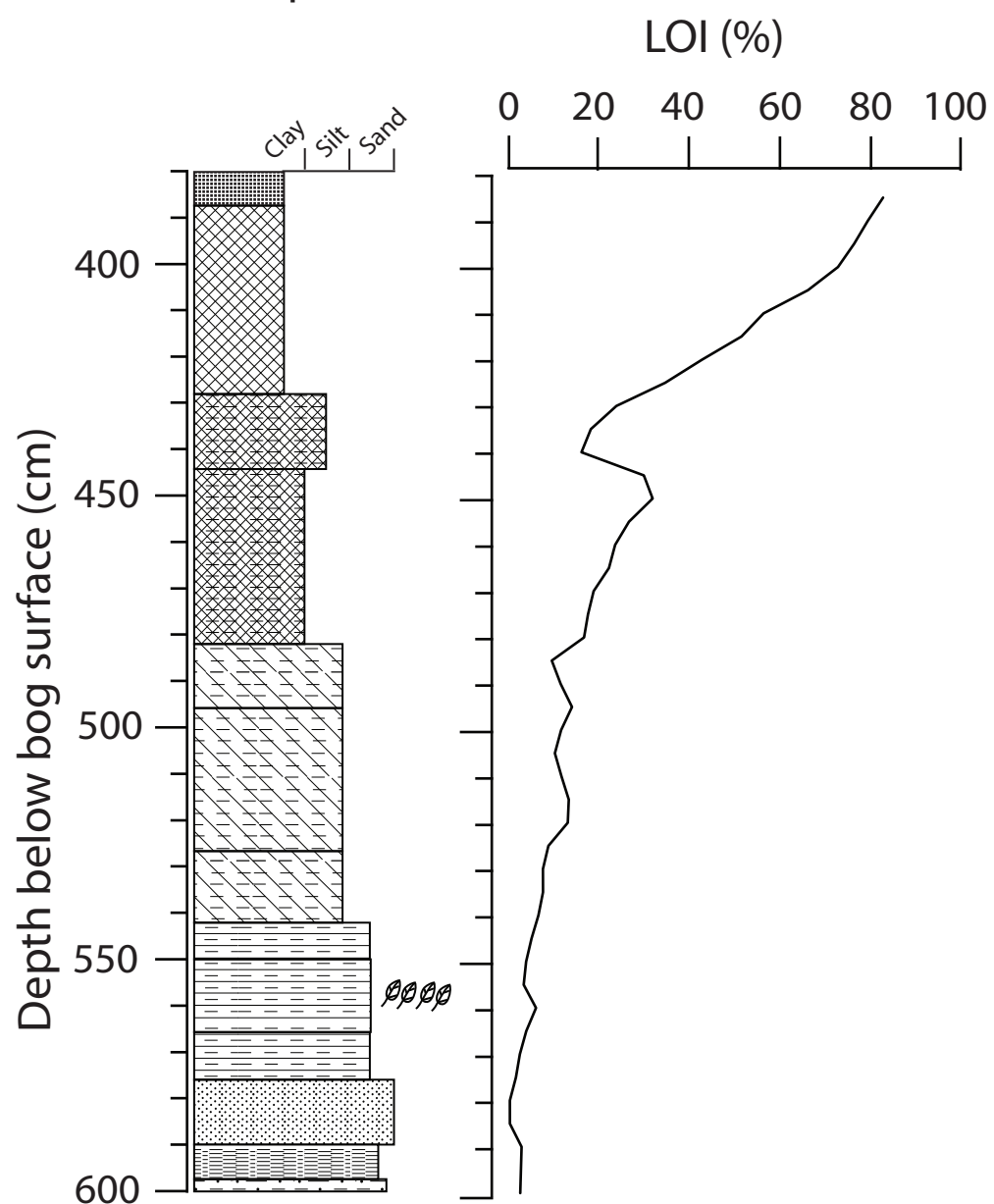
Table S2: Single-grain analyses of shards extracted from Atteköpsmosse core C-2011 between 508-509 cm and analysed at the Tephrochronology Analytical Unit University of Edinburgh (November 2015 and February 2016).

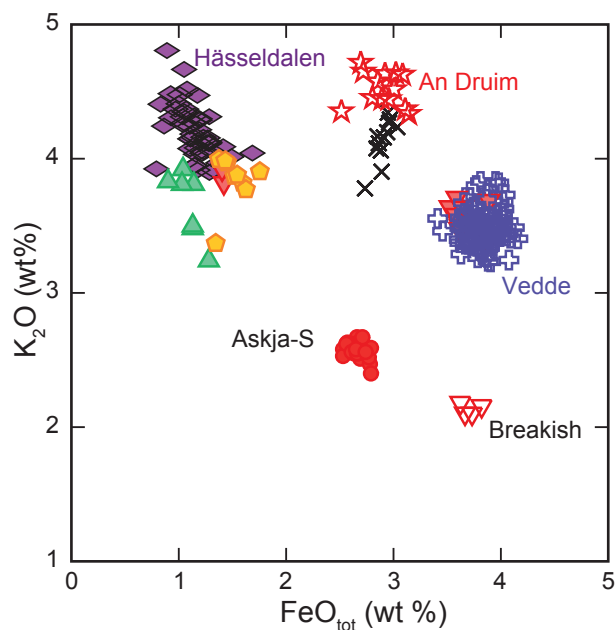
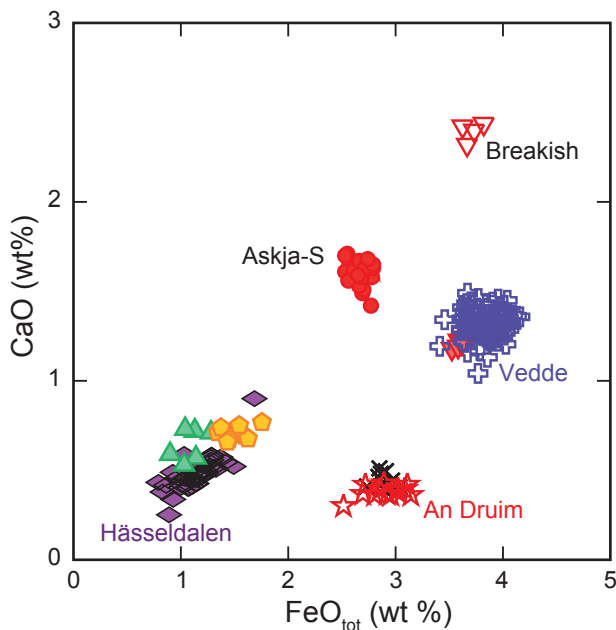
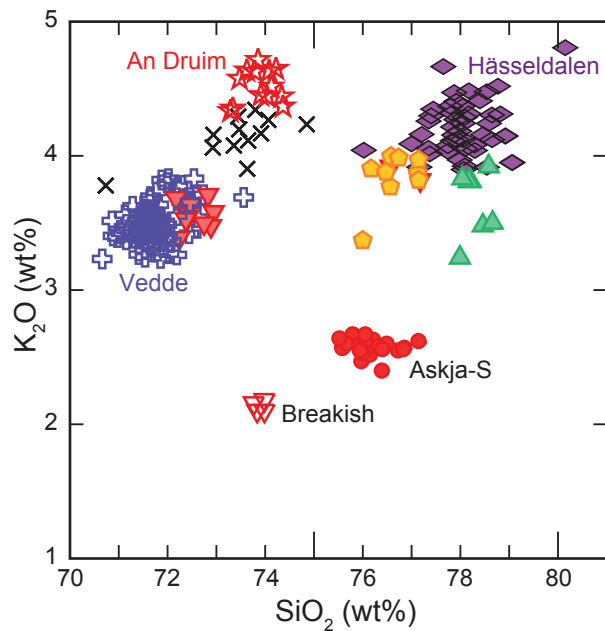
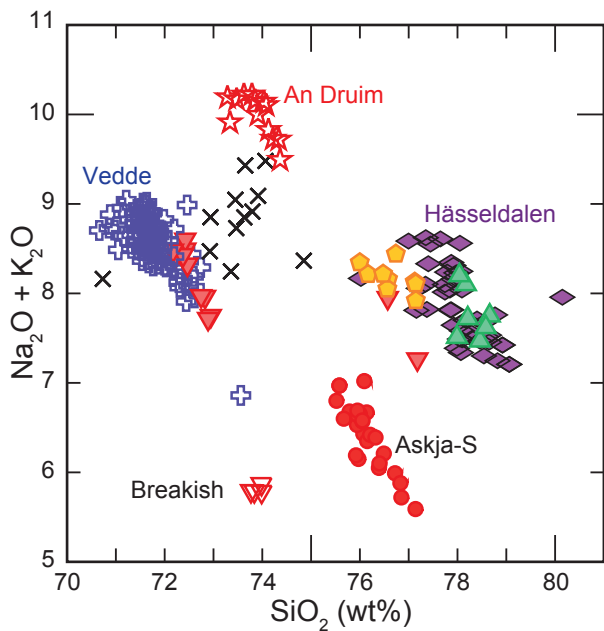


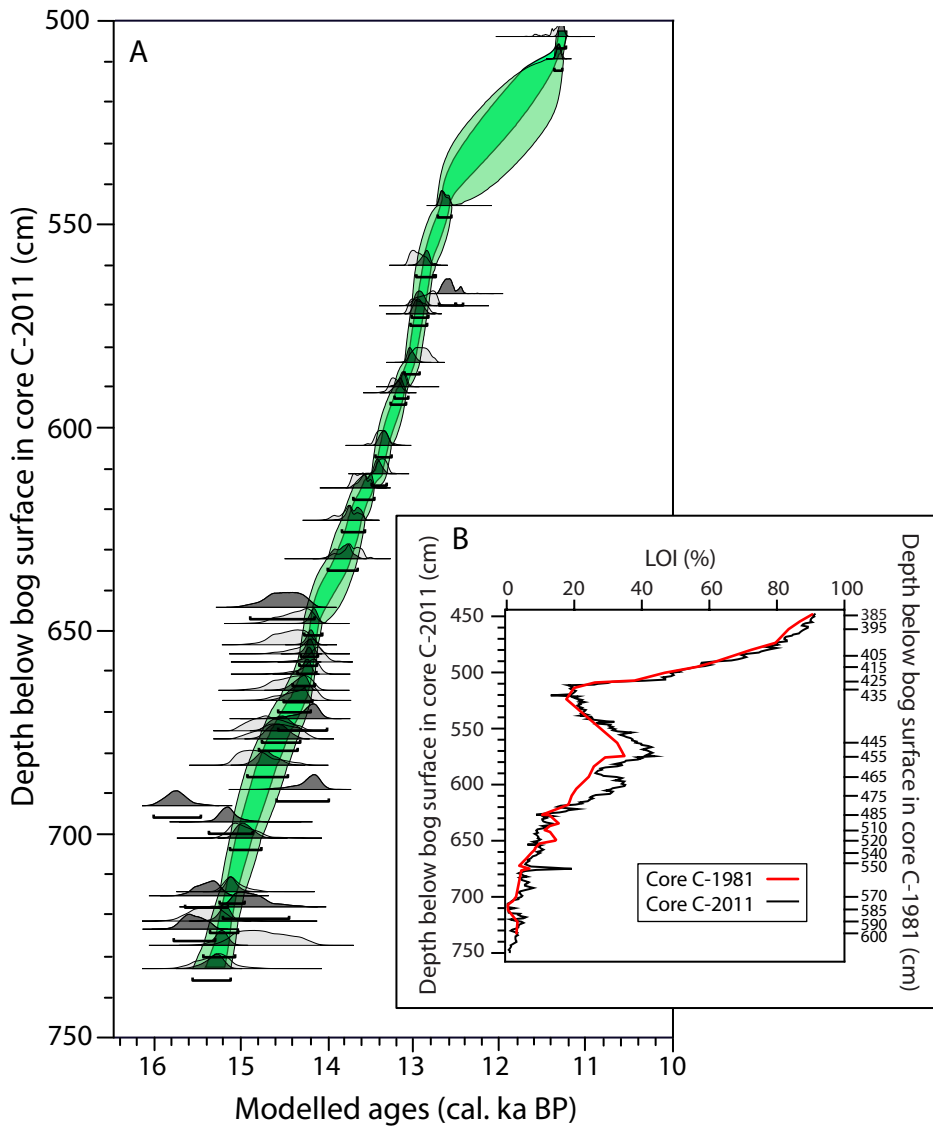
A Atteköpsmosse C-2011



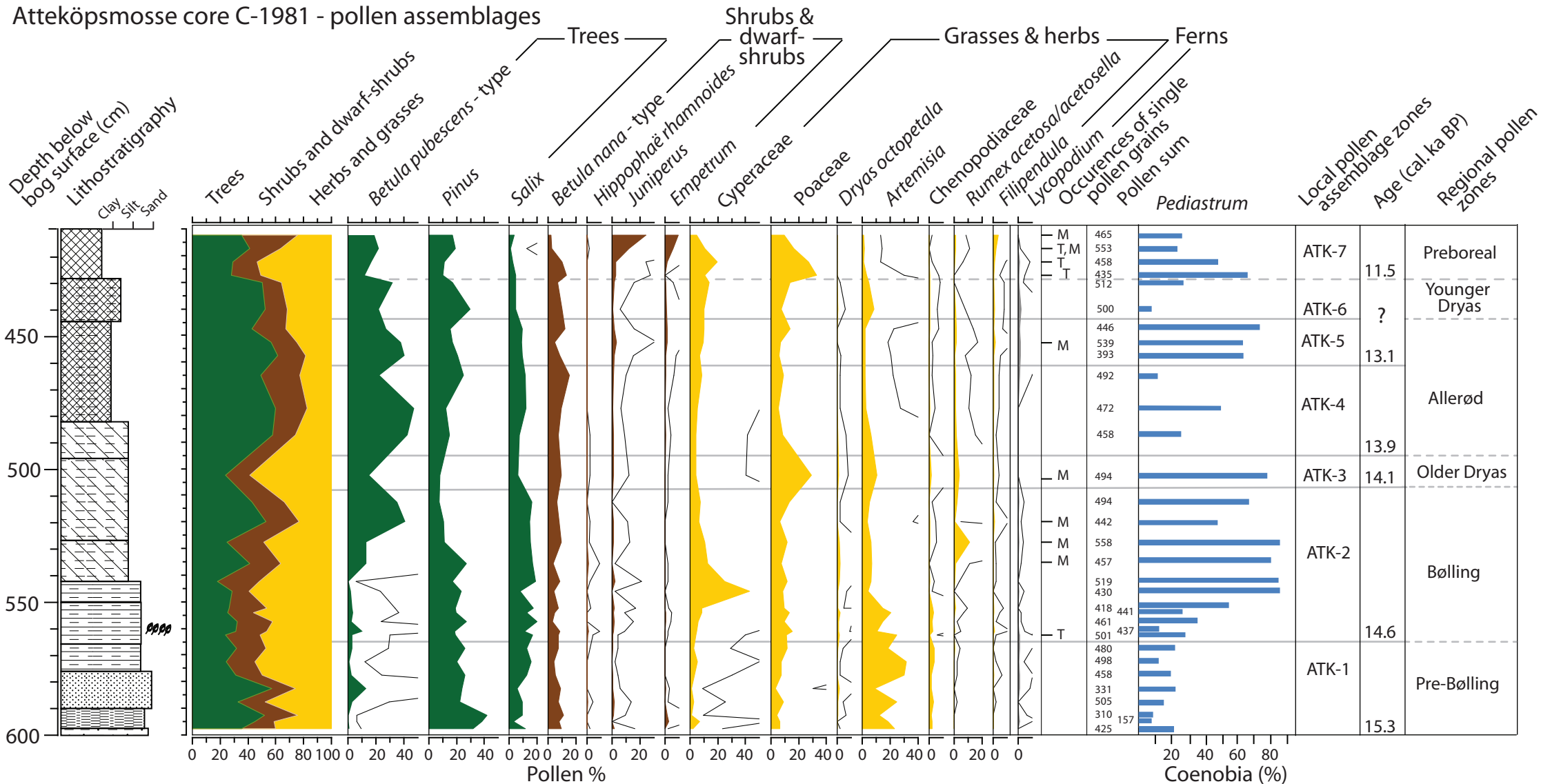
B Atteköpsmosse C-1981







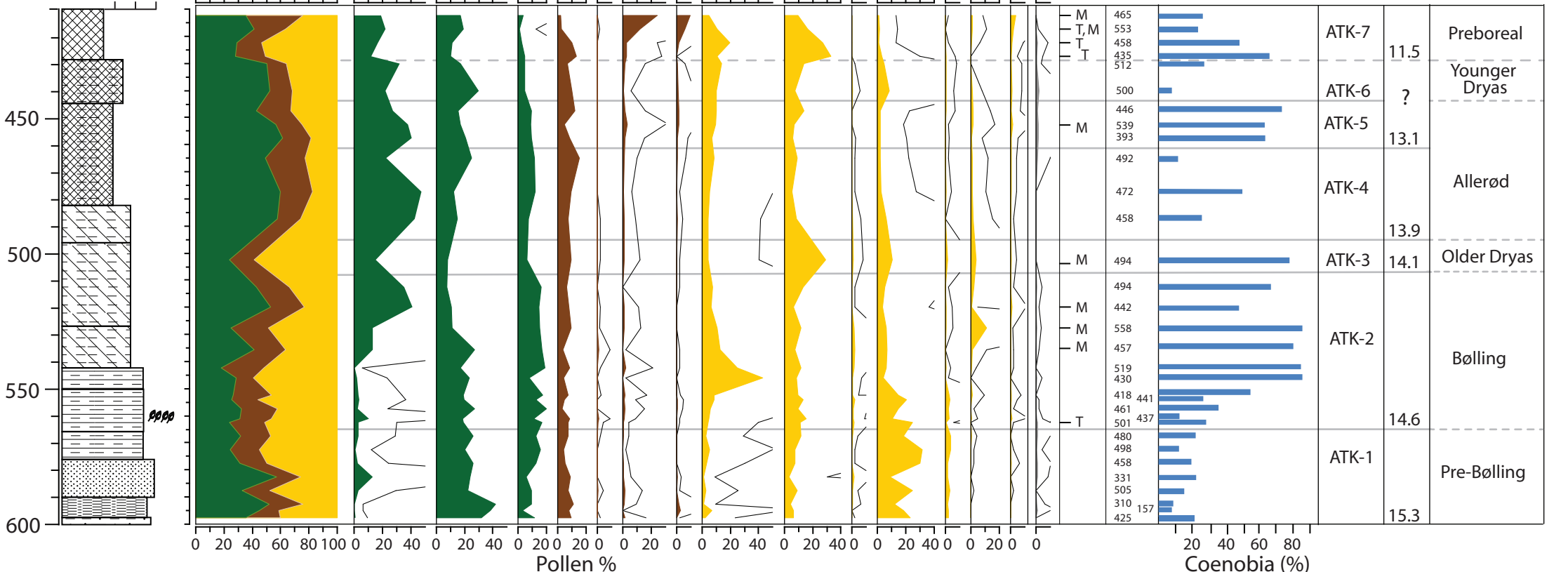
Atteköpsmossen core C-1981 - pollen assemblages



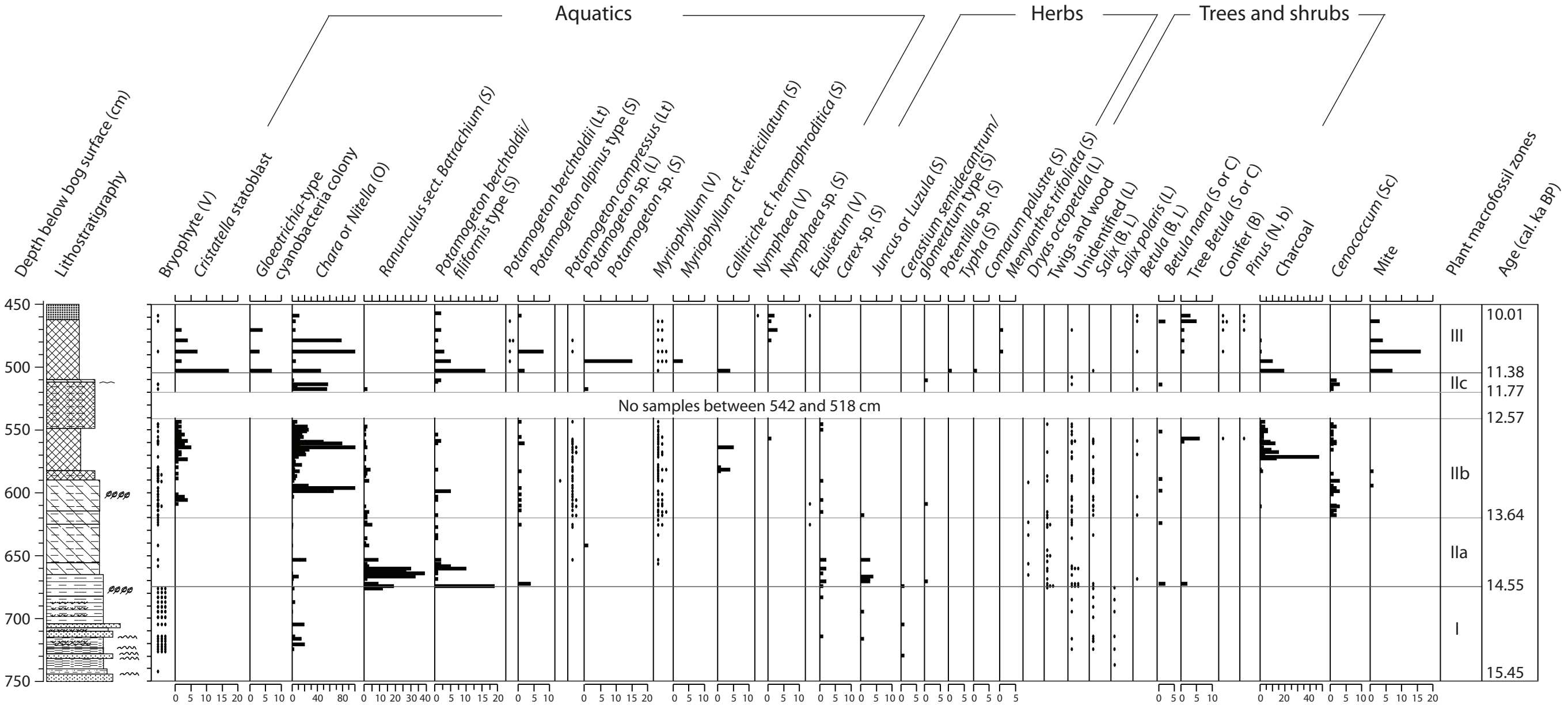
Depth below bog surface (cm)
Lithostratigraphy
Clay
Silt
Sand

Trees
Shrubs and dwarf-shrubs
Herbs and grasses
Betula pubescens - type
Pinus
Salix
Betula nana - type
Hippophaë rhamnoides
Juniperus
Empetrum
Cyperaceae
Poaceae
Dryas octopetala
Artemisia
Chenopodiaceae
Rumex acetosa/acetosella
Filipendula
Lycopodium
Occurrences of single pollen grains
Pollen sum

Local pollen assemblage zones
Age (cal. ka BP)
Regional pollen zones



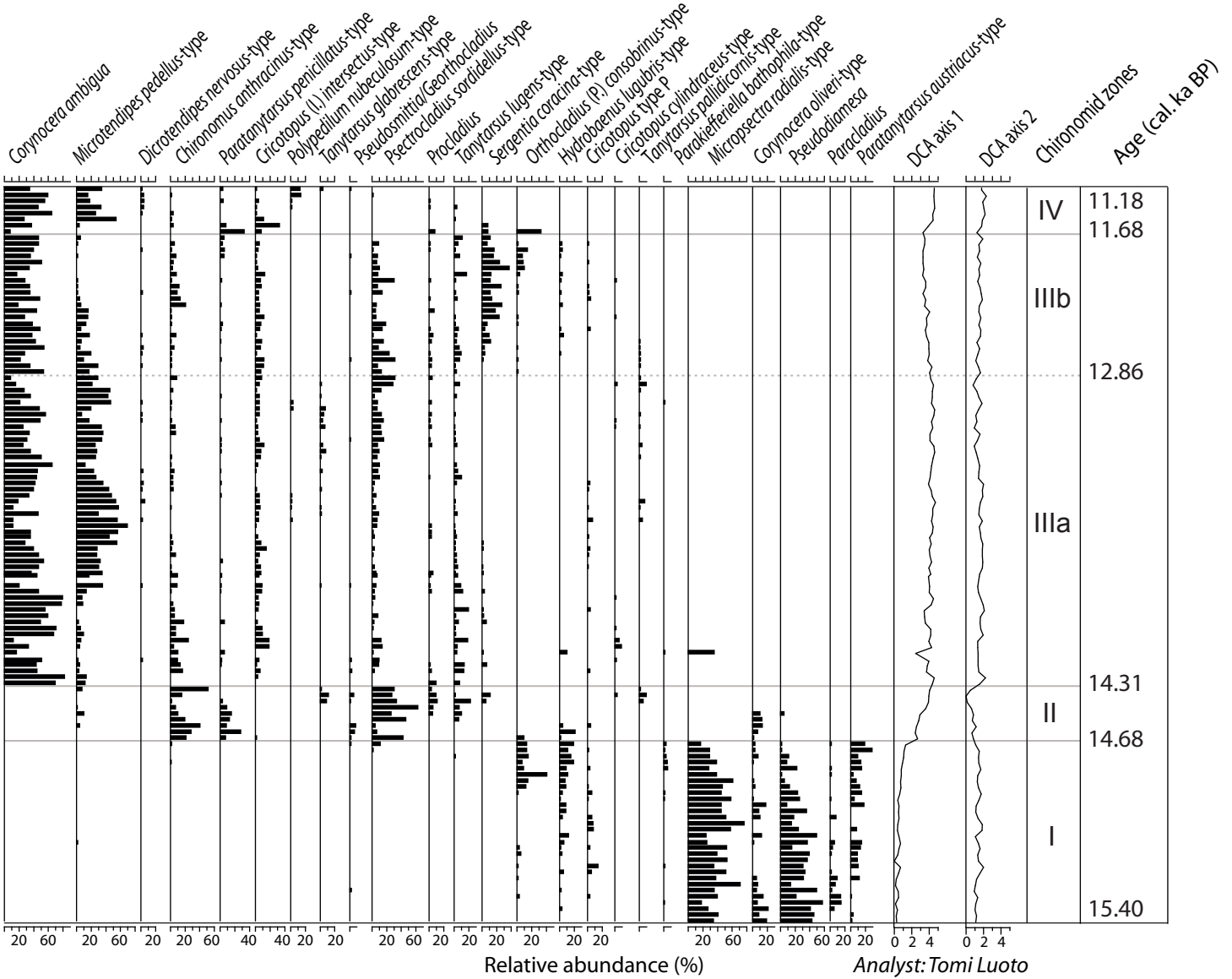
Atteköpsmosse core C-2011 - plant macrofossil remains



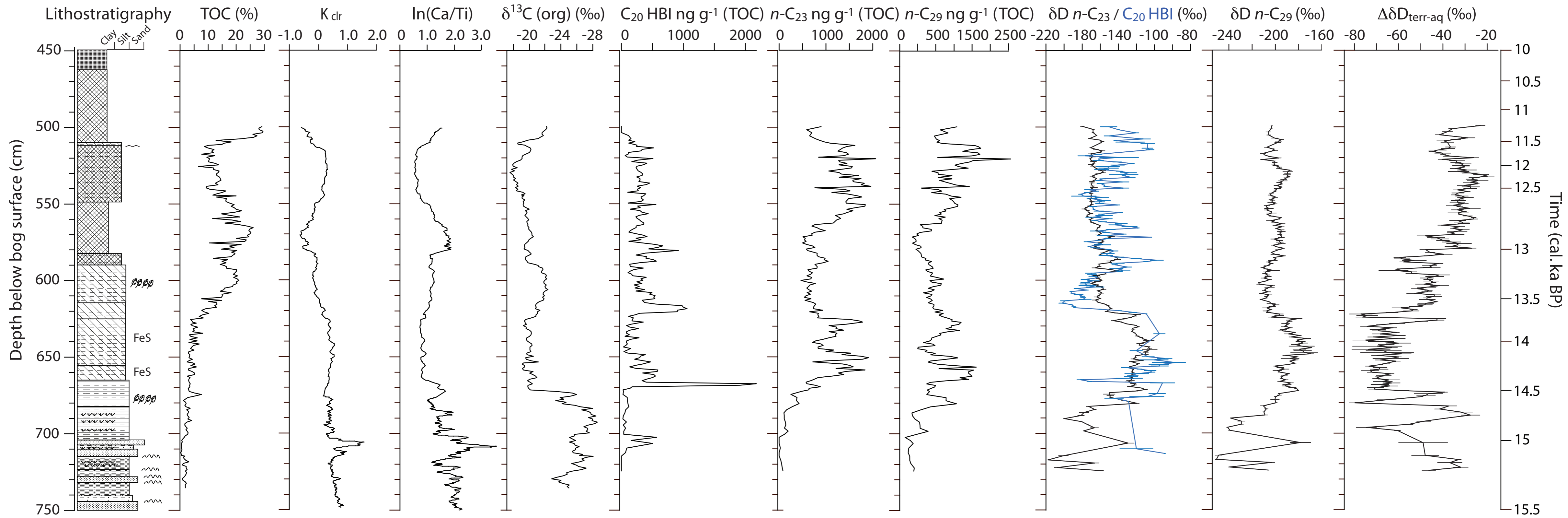
Analyst: Minna Väiranta

Atteköpsmossen core C-2011 - chironomid assemblages

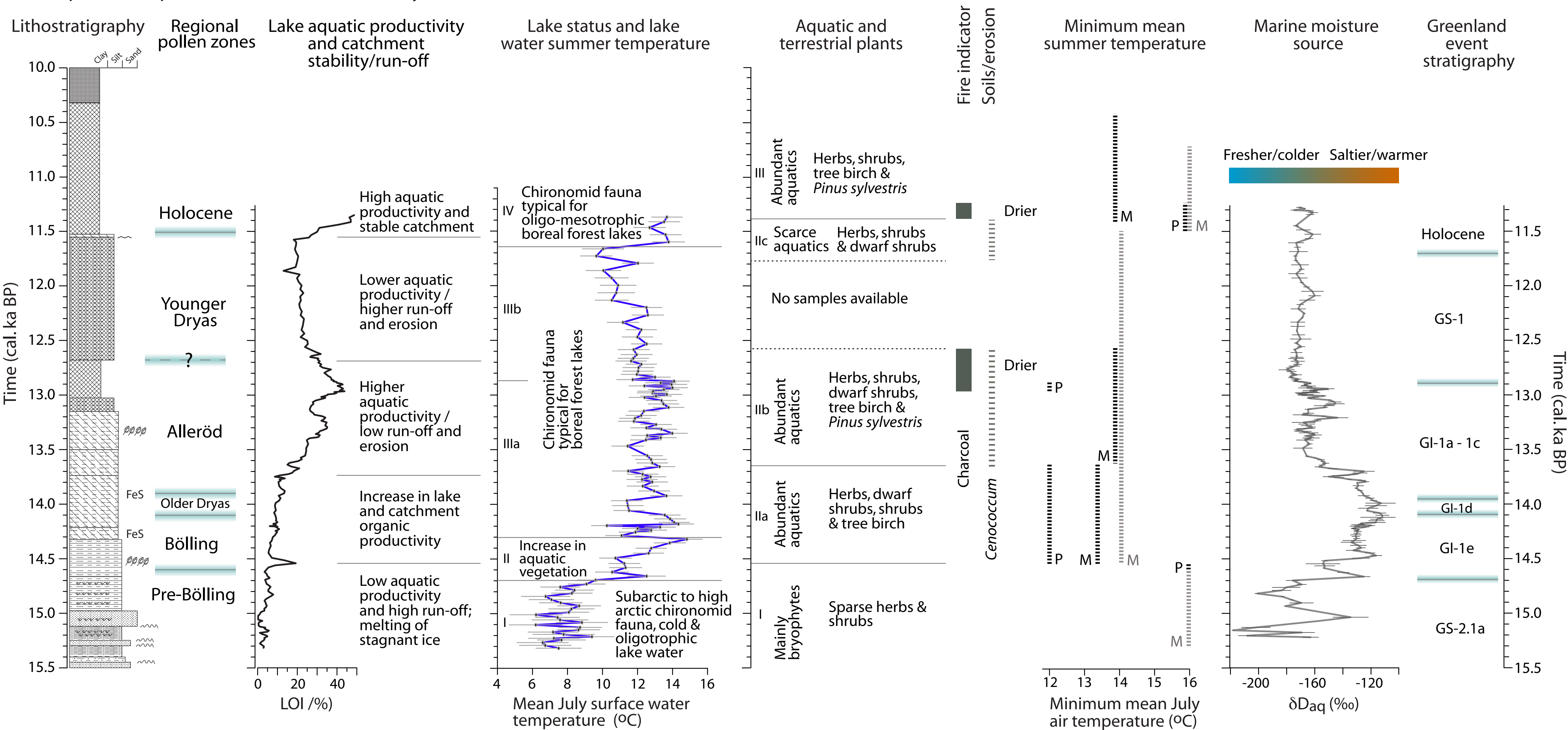
Depth below bog surface (cm)
Lithostratigraphy



Atteköpsmosse core C-2011



Atteköpsmosse - paleoenvironmental summary



Supporting Information for Wohlfarth et al. Climate and environment in southwest Sweden 15.5 – 11.3 cal. ka BP

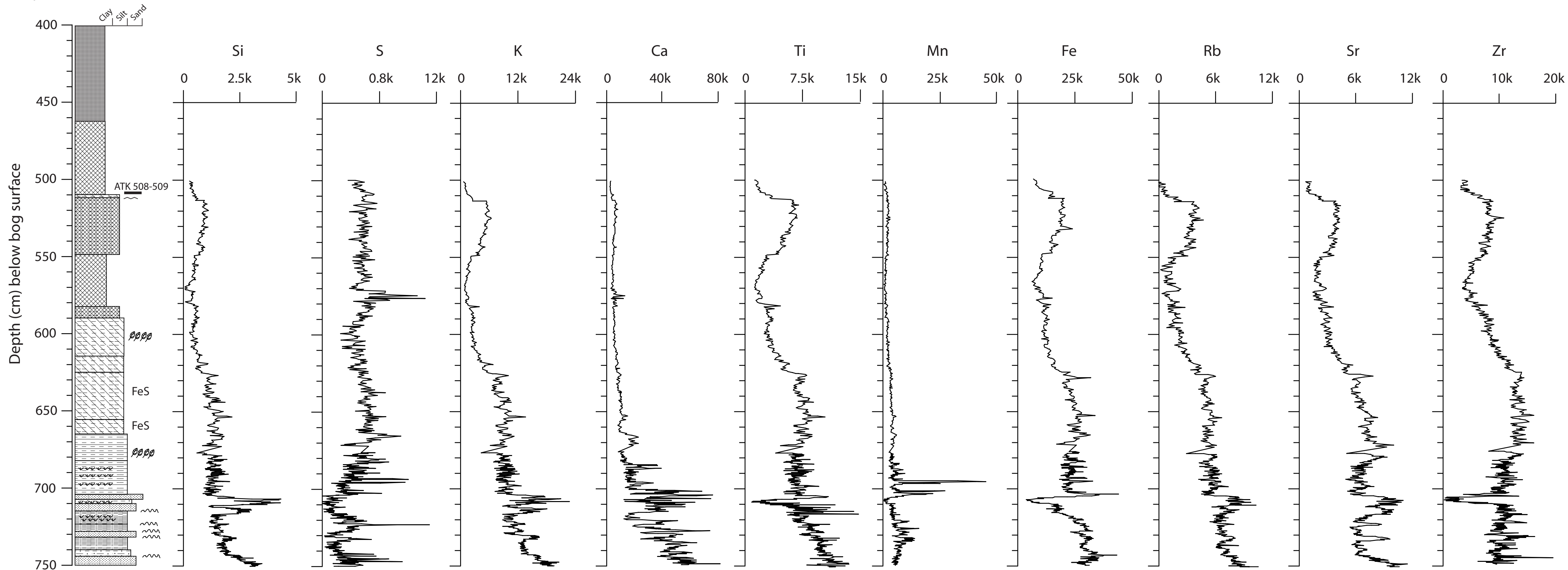
Fig. S1: Extended XRF data set for Atteköpsmosse core C-2011.

Fig. S2: Scatterplot of the δD n -C₂₃ (δD_{aq}) and δD n -C₂₉ (δD_{terr}) data sets for core C-2011.

Table S1: Lithostratigraphy of the Atteköpsmosse sediment profiles. Composite stratigraphy (A) of core C-2011 and (B) of core C-1981. s = sharp; vs = very sharp; g = gradual; vg = very gradual; LB = lower boundary.

Table S2: Single-grain analyses of shards extracted from Atteköpsmosse core C-2011 between 508-509 cm and analysed at the Tephrochronology Analytical Unit University of Edinburgh (November 2015 and February 2016).

Atteköpsmosse C-2011



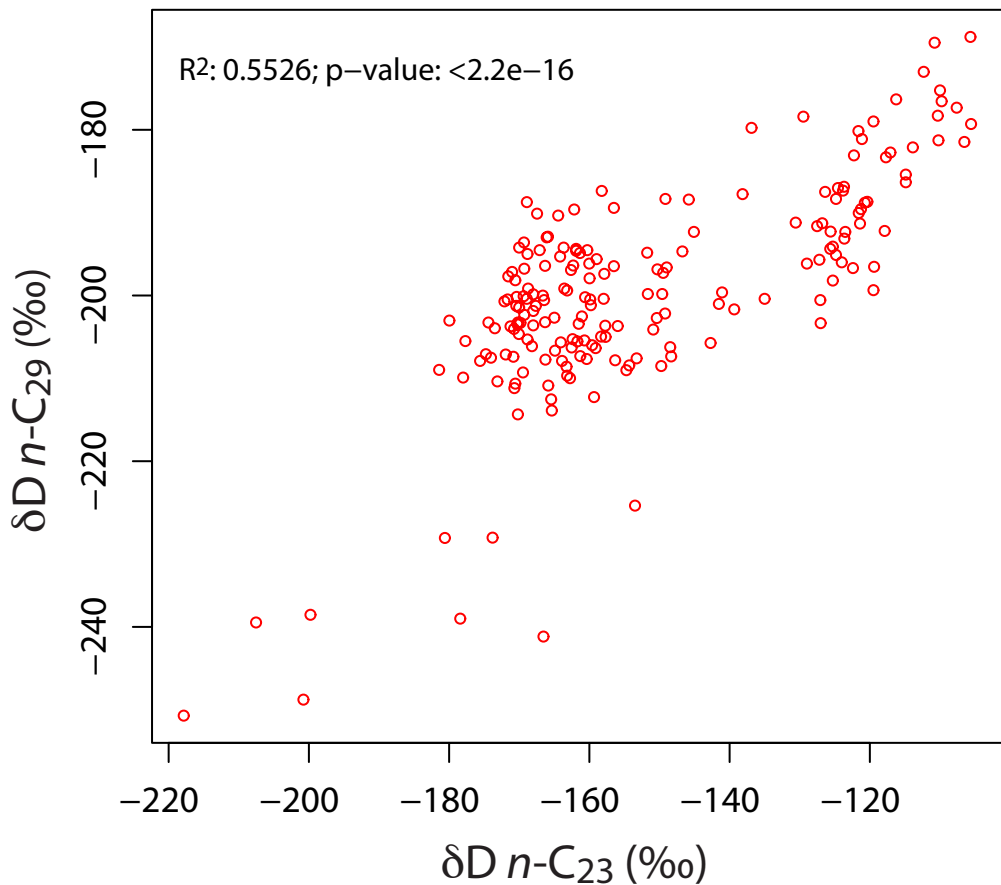


Table S1: Lithostratigraphy of the Atteköpsmosse sediment profiles. Composite stratigraphy (A) of core C-2011 and (B) of core C-1981. s = sharp; vs = very sharp; g = gradual; vg = very gradual; LB = lower boundary.

Depth (cm)	Sediment description
A. Core C-2011	
402 - 462	Dark brown coarse detritus gyttja or peat
462 - 510	Dark brown fine detritus gyttja, vgLB
510 - 511.5	Olive-brown to greyish silty gyttja, FeS coloring, disturbed LB
511.5 - 542	Olive-brown silty gyttja/algae gyttja, vgLB
542 - 549	Olive brown silty gyttja/algae gyttja with 6 thin organic layers, vgLB
549 - 582.5	Darker brown algae gyttja, vgLB; FeS spots
582.5 - 590	Brown silty gyttja/algae gyttja, vgLB
590 - 613.5	Brown silty gyttja, vgLB, visible organics or FeS spots
613.5 - 625	Slightly darker grey clayey silty gyttja
625 - 627.5	Brownish-grey clayey silty gyttja
627.5 - 629	Darker brown clayey silty gyttja; grey coloured lense at 629 cm
629 - 655	Brownish-grey clayey silty gyttja with some FeS stains, gLB
655 - 664	Brownish-orange clayey silty gyttja, FeS; moss layer or FeS layer at 657.5 cm, gLB
664 - 673	Olive brown - greyish gyttja silt, gLB in one core, very distinct LB in another core
673 - 677	Dark brown gyttja silt, gLB
677 - 682	Olive brown gyttja silt, gLB
682 - 702	Alternating layers of dark brown mosses and greyish-brown clayey gyttja silt; sLB marked by a band of FeS colored silt
702 - 714.5	714.5-710 cm: grey fine sand layer, sLB; 710-708 cm: grey sandy silt with mosses, sLB; 708-704 cm: grey coarse sand, fining upwards, sLB; 704-702 cm: grey silt. Many mosses in the sand layer of another core.
714.4 - 724	Alternating layers of dark brown mosses and greyish-brown clayey silt; gLB; 721-720 cm: grey sand layer
724 - 728	Brownish-grey clayey silt, organics, vsLB
728 - 731	Dark grey fine sand layer (1.5 cm) followed by grey-olive silt layer, sLB
731 - 740	Grey clayey silt with carbonate fragments, gLB
740 - 744.5	Grey silt with thin sand layers (1 mm), FeS banding, sLB
744.5 - 750	Grey fine sand layers
B. Core C-1981	
380 - 387	Dark green coarse detritus gyttja
387 - 427	Green fine detritus gyttja; coarse organic matter increases towards the top
427 - 444	Light grey to green silty gyttja
444 - 482	Brown greenish silty fine detritus gyttja
482 - 496	Light grey to green silty gyttja
496 - 527	Brown greenish silty gyttja
527 - 542	Light brown greenish silty gyttja
542 - 550	Light green gyttja silt

550 - 563	Grey to green gyttja silt with abundant coarse organic material
563 - 575	Greyish green gyttja silt
575 - 578	Grey fine sand, slightly organic
578 - 587	Greenish grey medium to fine sand
587 - 590	Greyish green organic fine to medium sand
590 - 598	Greyish green silt
598 - 600	Grey sandy silt

Table S2: Single-grain analyses of shards extracted from Attekopsmosse core C-2011 between 508 and 509 cm and analysed at the Tephrochronology Analytical Unit University of Edinburgh (November 2015 and February 2016).

Operating conditions:

CAMECA SX 100

Beam diameter 5 μm ;

Two sets of column conditions were utilised within the EPMA analysis.

Firstly Na, Al, Si, K, Ca, Mg and Fe were determined using an accelerating voltage of 15 kV and a beam current of 10 nA. P, Ti and Mn were then determined using an accelerating voltage of 15 kV and a beam current of 10 nA. Counting times were 20 s at the peak position and 10 s for background for all elements except T

15 kV and a beam current of 2 nA.

beam current of 80 nA. A 5 μm electron beam diameter was used throughout.

times except Ti (30 s and 15 s), Mn (50 s and 40 s) and Fe (40 s and 20 s).

NON NORMALISED DATA

DataSet/Point	SiO2	TiO2	Al2O3	FeO	MnO
ATK 508-09 cm_nov	75.38	0.11	11.48	1.08	0.06
ATK 508-09 cm_nov	75.61	0.12	11.06	1.09	0.05
ATK 508-09 cm_nov	75.85	0.11	11.35	1.01	0.05
ATK 508-09 cm_nov	75.42	0.11	11.68	1.10	0.05
ATK 508-09_feb	74.83	0.07	11.47	0.98	0.05
ATK 508-09_feb	74.63	0.08	11.53	0.86	0.04
ATK 508-09_feb	74.72	0.11	11.72	1.23	0.05
Mean	75.21	0.10	11.47	1.05	0.05
Stdev	0.44	0.02	0.20	0.11	0.00

MgO	CaO	Na2O	K2O	P2O5	Total
0.09	0.70	3.84	3.34	0.01	96.07
0.06	0.69	4.08	3.37	0.01	96.12
0.09	0.71	3.57	3.79	0.01	96.53
0.06	0.55	3.77	3.68	0.00	96.43
0.04	0.51	4.11	3.65	0.01	95.73
0.07	0.57	4.17	3.67	0.00	95.62
0.09	0.68	4.09	3.11	0.01	95.81
0.07	0.63	3.95	3.51	0.01	96.05
0.02	0.07	0.21	0.23	0.00	0.32

SECONDARY STANDARD DATA from Nov 2015 and Feb 2016 (i.e. during analysis of ATK 508-0)

SiO2	TiO2	Al2O3	FeO	MnO	MgO	CaO
74.57	0.08	12.81	1.57	0.07	0.05	0.79
74.75	0.08	12.98	1.58	0.07	0.05	0.81
74.99	0.08	13.05	1.37	0.06	0.02	0.82
74.36	0.08	12.82	1.49	0.08	0.01	0.79
73.82	0.07	12.60	1.31	0.07	0.04	0.79
74.56	0.08	13.12	1.64	0.08	0.06	0.70
73.52	0.08	12.88	1.45	0.06	0.04	0.76
74.37	0.08	12.89	1.49	0.07	0.04	0.78
0.52	0.00	0.17	0.12	0.01	0.02	0.04
73.94	0.08	13.16	1.57	0.06	0.03	0.75
74.80	0.08	12.95	1.62	0.07	0.05	0.75
74.31	0.08	13.15	1.54	0.08	0.06	0.75
74.99	0.08	12.78	1.67	0.08	0.05	0.76
73.36	0.08	13.03	1.52	0.06	0.06	0.72
73.87	0.09	13.08	1.48	0.06	0.05	0.74
73.51	0.09	12.96	1.66	0.07	0.07	0.73
75.02	0.08	13.09	1.51	0.07	0.06	0.75
73.43	0.07	12.83	1.55	0.06	0.08	0.70
73.77	0.08	13.11	1.38	0.07	0.06	0.78
74.23	0.07	12.92	1.72	0.08	0.05	0.76
74.37	0.08	13.09	1.61	0.06	0.04	0.77
74.70	0.08	13.14	1.66	0.07	0.02	0.78
74.85	0.08	13.05	1.57	0.07	0.04	0.79
72.92	0.08	12.88	1.54	0.08	0.03	0.77
74.42	0.08	13.48	1.59	0.07	0.04	0.71
74.16	0.08	13.04	1.57	0.07	0.05	0.75
0.64	0.00	0.16	0.08	0.01	0.02	0.03
73.14	0.05	12.77	1.49	0.04	0.02	0.68
75.06	0.10	13.45	1.61	0.10	0.06	0.79
53.57	2.28	13.27	12.62	0.20	3.69	7.11
54.47	2.31	13.23	12.65	0.20	3.52	7.20
55.66	2.28	13.09	12.16	0.20	3.55	7.12
55.11	2.29	13.00	12.75	0.19	3.54	7.06
54.76	2.28	13.02	12.64	0.19	3.46	6.96
55.22	2.27	13.53	12.22	0.20	3.48	7.18
54.76	2.29	13.14	12.65	0.21	3.49	7.24
54.28	2.28	13.26	12.89	0.21	3.57	6.99

54.73	2.29	13.19	12.57	0.20	3.54	7.11
0.64	0.01	0.17	0.25	0.01	0.07	0.10

53.93	2.29	13.47	11.97	0.20	3.64	7.13
54.79	2.28	13.30	12.54	0.20	3.54	7.31
53.69	2.27	13.30	12.92	0.20	3.64	7.12
53.49	2.27	13.60	12.24	0.19	3.73	7.38
54.75	2.28	13.38	12.80	0.20	3.69	7.50
54.15	2.28	13.72	12.63	0.21	3.71	7.19
54.13	2.28	13.29	12.19	0.20	3.55	7.34
54.52	2.26	13.30	12.43	0.18	3.59	7.30
54.78	2.28	13.40	12.48	0.20	3.69	7.38
54.45	2.28	13.53	12.51	0.21	3.62	7.12
53.89	2.29	13.36	12.66	0.19	3.63	7.02
54.03	2.28	13.08	12.53	0.20	3.57	7.00
54.44	2.28	13.34	12.23	0.22	3.52	7.31
53.68	2.29	13.54	12.54	0.22	3.34	7.27
54.63	2.28	13.45	12.68	0.20	3.73	7.27
55.18	2.30	13.15	11.98	0.20	3.67	6.92
54.77	2.28	13.46	12.11	0.20	3.68	7.45
53.92	2.27	13.38	12.37	0.20	3.45	7.07
55.38	2.29	12.89	11.91	0.20	3.43	7.18
54.77	2.27	13.32	13.10	0.20	3.58	7.14

54.37	2.28	13.36	12.44	0.20	3.60	7.22
0.51	0.01	0.18	0.31	0.01	0.10	0.15

53.30	2.21	13.30	12.42	N/A	3.54	7.01
55.00	2.31	13.70	14.00	N/A	3.64	7.23

f ATK 508-09cm)

Recommended values for the Lipari from Kuehn et al. (2011) and

Na2O	K2O	P2O5	Total	Comment
4.03	5.23	0.02	99.22	Lipari
4.06	5.15	0.00	99.51	Lipari
3.88	5.35	0.01	99.62	Lipari
3.84	5.24	0.01	98.72	Lipari
3.87	5.17	0.00	97.74	Lipari
3.82	5.08	0.00	99.14	Lipari
3.81	5.18	0.01	97.79	Lipari
3.90	5.20	0.01	98.82	AVERAGE
0.10	0.08	0.01	0.78	Stdev
4.21	5.21	0.01	99.03	Lipari
3.98	5.20	0.01	99.52	Lipari
4.38	5.20	0.00	99.54	Lipari
4.12	5.19	0.01	99.73	Lipari
4.07	5.09	0.01	98.00	Lipari
4.10	5.21	0.00	98.68	Lipari
4.17	5.15	0.00	98.41	Lipari
3.96	5.44	0.01	99.99	Lipari
4.18	5.17	0.00	98.07	Lipari
4.17	5.11	0.00	98.52	Lipari
4.09	5.15	0.00	99.06	Lipari
4.17	5.33	0.01	99.51	Lipari
4.33	5.35	0.00	100.13	Lipari
3.98	5.17	0.00	99.61	Lipari
4.20	5.26	0.00	97.76	Lipari
4.07	5.24	0.00	99.69	Lipari
4.14	5.22	0.00	99.08	AVERAGE
0.12	0.09	0.01	0.75	Stdev
3.78	4.87	-0.01		
4.34	5.39	0.02		
3.08	1.85	0.34	98.00	BCR2g
2.66	1.79	0.36	98.40	BCR2g
3.22	1.84	0.34	99.46	BCR2g
3.08	1.75	0.32	99.08	BCR2g
3.02	1.80	0.34	98.48	BCR2g
3.16	1.81	0.34	99.41	BCR2g
3.24	1.79	0.34	99.15	BCR2g
3.13	1.84	0.32	98.77	BCR2g

3.07	1.81	0.34	98.84 AVERAGE
0.18	0.03	0.01	0.52 St dev

3.30	1.75	0.34	98.02 BCR2g
3.30	1.79	0.38	99.44 BCR2g
3.15	1.83	0.35	98.46 BCR2g
3.30	1.80	0.35	98.36 BCR2g
2.29	1.83	0.36	99.06 BCR2g
2.83	1.82	0.35	98.89 BCR2g
3.30	1.78	0.29	98.35 BCR2g
3.38	1.77	0.28	99.02 BCR2g
3.15	1.89	0.29	99.53 BCR2g
3.14	1.73	0.31	98.89 BCR2g
3.10	1.90	0.31	98.35 BCR2g
3.28	1.89	0.38	98.24 BCR2g
3.41	1.86	0.36	98.97 BCR2g
3.23	1.79	0.29	98.20 BCR2g
3.09	1.89	0.30	99.51 BCR2g
3.32	1.80	0.31	98.82 BCR2g
3.52	1.73	0.31	99.50 BCR2g
3.41	1.89	0.32	98.27 BCR2g
3.01	1.89	0.29	98.49 BCR2g
3.31	1.73	0.32	99.73 BCR2g

3.19	1.82	0.32	98.80 AVERAGE
0.26	0.06	0.03	0.52 St dev

3.05	1.74	0.33	
3.27	1.84	0.37	98.49

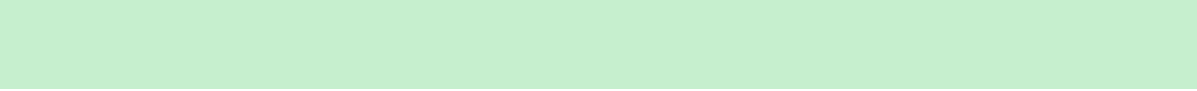
(2011) and for BCR2G from http://minerals.cr.usgs.gov/geo_chem_stand/basaltbcr2.html (accessed 12/06/13) are shown

Date

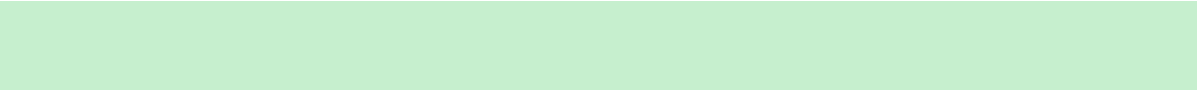
07/11/2015 09:32
07/11/2015 09:37
07/11/2015 09:43
07/11/2015 19:56
07/11/2015 20:01
07/11/2015 20:06
07/11/2015 20:12

29/02/2016 11:05
29/02/2016 11:10
29/02/2016 11:15
29/02/2016 19:07
29/02/2016 19:12
29/02/2016 19:18
29/02/2016 20:11
29/02/2016 20:16
01/03/2016 03:33
01/03/2016 03:38
01/03/2016 03:44
01/03/2016 03:49
01/03/2016 03:54
01/03/2016 03:59
01/03/2016 04:05
01/03/2016 04:10

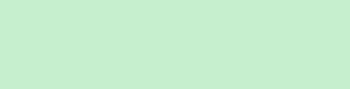
07/11/2015 09:49
07/11/2015 09:54
07/11/2015 09:59
07/11/2015 19:29
07/11/2015 19:34
07/11/2015 19:39
07/11/2015 19:45
07/11/2015 19:50



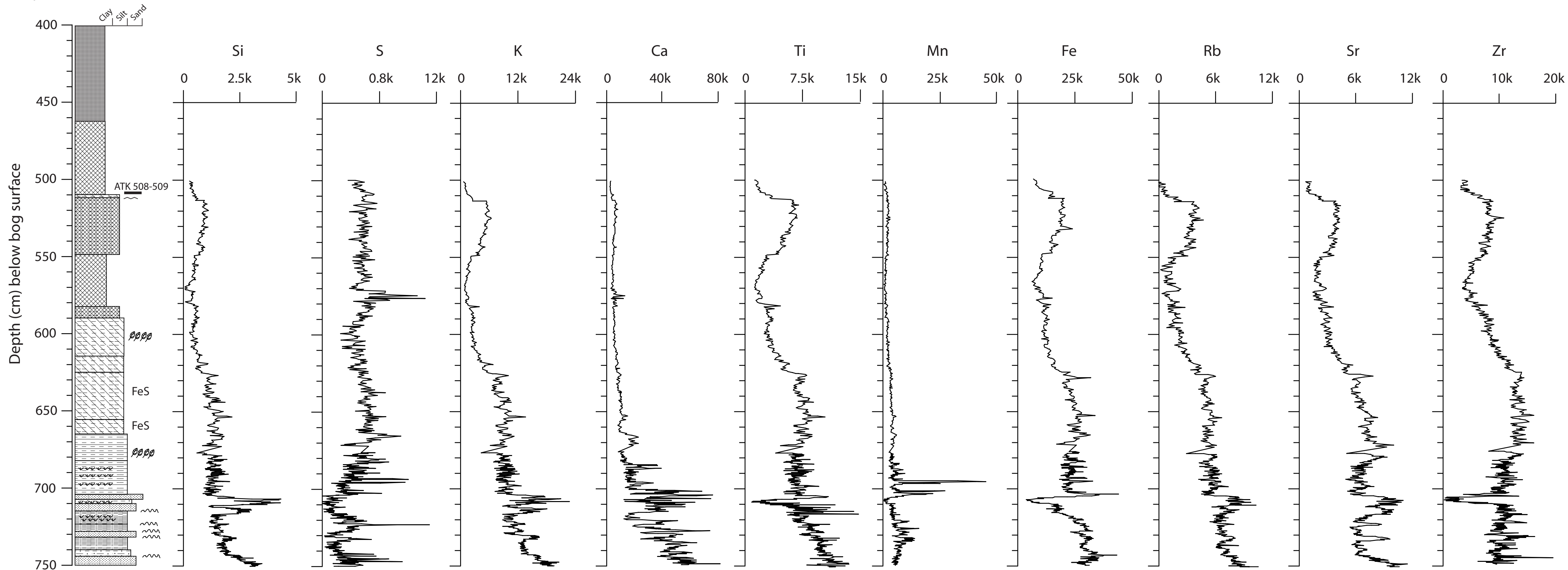
29/02/2016 10:49
29/02/2016 10:54
29/02/2016 10:59
29/02/2016 11:26
29/02/2016 11:31
29/02/2016 11:36
29/02/2016 19:28
29/02/2016 19:33
29/02/2016 19:39
29/02/2016 19:44
29/02/2016 19:50
29/02/2016 19:57
29/02/2016 20:04
01/03/2016 02:56
01/03/2016 03:02
01/03/2016 03:07
01/03/2016 03:12
01/03/2016 03:17
01/03/2016 03:23
01/03/2016 03:28



accessed 12/06/13) are shown in red.



Atteköpsmosse C-2011



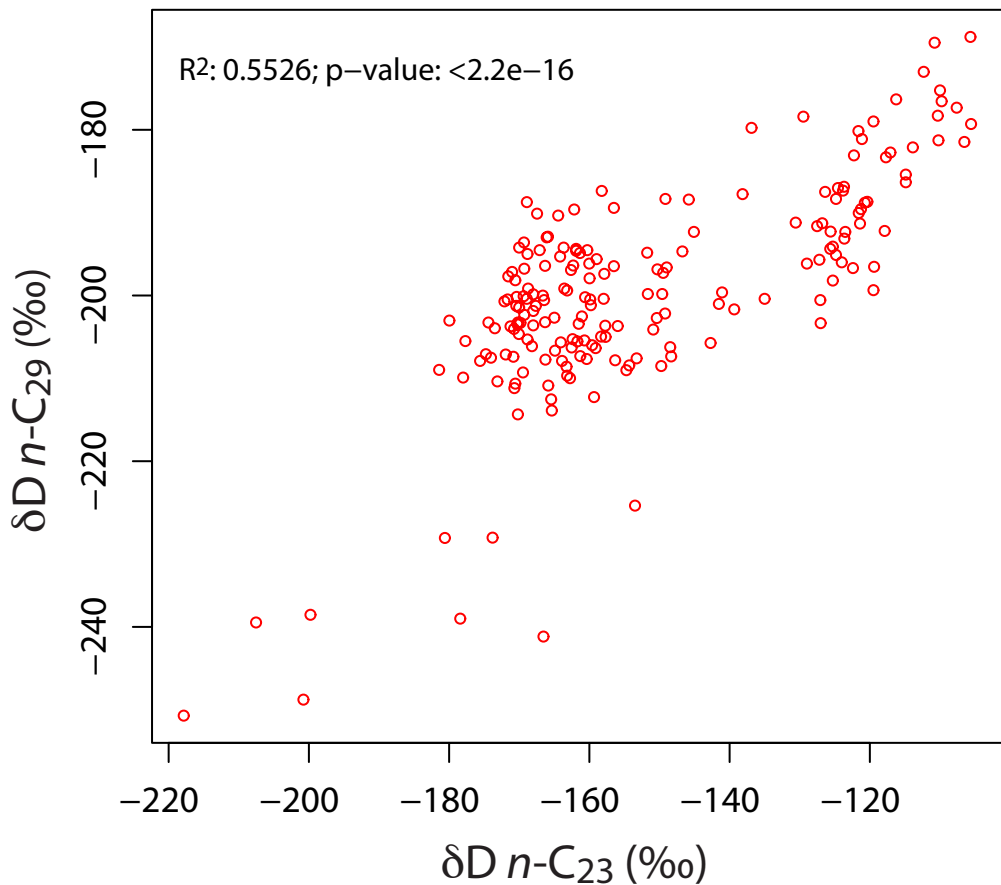


Table S1: Lithostratigraphy of the Atteköpsmosse sediment profiles. Composite stratigraphy (A) of core C-2011 and (B) of core C-1981. s = sharp; vs = very sharp; g = gradual; vg = very gradual; LB = lower boundary.

Depth (cm)	Sediment description
A. Core C-2011	
402 - 462	Dark brown coarse detritus gyttja or peat
462 - 510	Dark brown fine detritus gyttja, vgLB
510 - 511.5	Olive-brown to greyish silty gyttja, FeS coloring, disturbed LB
511.5 - 542	Olive-brown silty gyttja/algae gyttja, vgLB
542 - 549	Olive brown silty gyttja/algae gyttja with 6 thin organic layers, vgLB
549 - 582.5	Darker brown algae gyttja, vgLB; FeS spots
582.5 - 590	Brown silty gyttja/algae gyttja, vgLB
590 - 613.5	Brown silty gyttja, vgLB, visible organics or FeS spots
613.5 - 625	Slightly darker grey clayey silty gyttja
625 - 627.5	Brownish-grey clayey silty gyttja
627.5 - 629	Darker brown clayey silty gyttja; grey coloured lense at 629 cm
629 - 655	Brownish-grey clayey silty gyttja with some FeS stains, gLB
655 - 664	Brownish-orange clayey silty gyttja, FeS; moss layer or FeS layer at 657.5 cm, gLB
664 - 673	Olive brown - greyish gyttja silt, gLB in one core, very distinct LB in another core
673 - 677	Dark brown gyttja silt, gLB
677 - 682	Olive brown gyttja silt, gLB
682 - 702	Alternating layers of dark brown mosses and greyish-brown clayey gyttja silt; sLB marked by a band of FeS colored silt
702 - 714.5	714.5-710 cm: grey fine sand layer, sLB; 710-708 cm: grey sandy silt with mosses, sLB; 708-704 cm: grey coarse sand, fining upwards, sLB; 704-702 cm: grey silt. Many mosses in the sand layer of another core.
714.4 - 724	Alternating layers of dark brown mosses and greyish-brown clayey silt; gLB; 721-720 cm: grey sand layer
724 - 728	Brownish-grey clayey silt, organics, vsLB
728 - 731	Dark grey fine sand layer (1.5 cm) followed by grey-olive silt layer, sLB
731 - 740	Grey clayey silt with carbonate fragments, gLB
740 - 744.5	Grey silt with thin sand layers (1 mm), FeS banding, sLB
744.5 - 750	Grey fine sand layers
B. Core C-1981	
380 - 387	Dark green coarse detritus gyttja
387 - 427	Green fine detritus gyttja; coarse organic matter increases towards the top
427 - 444	Light grey to green silty gyttja
444 - 482	Brown greenish silty fine detritus gyttja
482 - 496	Light grey to green silty gyttja
496 - 527	Brown greenish silty gyttja
527 - 542	Light brown greenish silty gyttja
542 - 550	Light green gyttja silt

550 - 563	Grey to green gyttja silt with abundant coarse organic material
563 - 575	Greyish green gyttja silt
575 - 578	Grey fine sand, slightly organic
578 - 587	Greenish grey medium to fine sand
587 - 590	Greyish green organic fine to medium sand
590 - 598	Greyish green silt
598 - 600	Grey sandy silt

Table S2: Single-grain analyses of shards extracted from Attekopsmosse core C-2011 between 508 and 509 cm and analysed at the Tephrochronology Analytical Unit University of Edinburgh (November 2015 and February 2016).

Operating conditions:

CAMECA SX 100

Beam diameter 5 μm ;

Two sets of column conditions were utilised within the EPMA analysis.

Firstly Na, Al, Si, K, Ca, Mg and Fe were determined using an accelerating voltage of 15 kV and a beam current of 10 nA. P, Ti and Mn were then determined using an accelerating voltage of 15 kV and a beam current of 10 nA. Counting times were 20 s at the peak position and 10 s for background for all elements except T

15 kV and a beam current of 2 nA.

beam current of 80 nA. A 5 μm electron beam diameter was used throughout.

times except Ti (30 s and 15 s), Mn (50 s and 40 s) and Fe (40 s and 20 s).

NON NORMALISED DATA

DataSet/Point	SiO2	TiO2	Al2O3	FeO	MnO
ATK 508-09 cm_nov	75.38	0.11	11.48	1.08	0.06
ATK 508-09 cm_nov	75.61	0.12	11.06	1.09	0.05
ATK 508-09 cm_nov	75.85	0.11	11.35	1.01	0.05
ATK 508-09 cm_nov	75.42	0.11	11.68	1.10	0.05
ATK 508-09_feb	74.83	0.07	11.47	0.98	0.05
ATK 508-09_feb	74.63	0.08	11.53	0.86	0.04
ATK 508-09_feb	74.72	0.11	11.72	1.23	0.05
Mean	75.21	0.10	11.47	1.05	0.05
Stdev	0.44	0.02	0.20	0.11	0.00

MgO	CaO	Na2O	K2O	P2O5	Total
0.09	0.70	3.84	3.34	0.01	96.07
0.06	0.69	4.08	3.37	0.01	96.12
0.09	0.71	3.57	3.79	0.01	96.53
0.06	0.55	3.77	3.68	0.00	96.43
0.04	0.51	4.11	3.65	0.01	95.73
0.07	0.57	4.17	3.67	0.00	95.62
0.09	0.68	4.09	3.11	0.01	95.81
0.07	0.63	3.95	3.51	0.01	96.05
0.02	0.07	0.21	0.23	0.00	0.32

SECONDARY STANDARD DATA from Nov 2015 and Feb 2016 (i.e. during analysis of ATK 508-0)

SiO2	TiO2	Al2O3	FeO	MnO	MgO	CaO
74.57	0.08	12.81	1.57	0.07	0.05	0.79
74.75	0.08	12.98	1.58	0.07	0.05	0.81
74.99	0.08	13.05	1.37	0.06	0.02	0.82
74.36	0.08	12.82	1.49	0.08	0.01	0.79
73.82	0.07	12.60	1.31	0.07	0.04	0.79
74.56	0.08	13.12	1.64	0.08	0.06	0.70
73.52	0.08	12.88	1.45	0.06	0.04	0.76
74.37	0.08	12.89	1.49	0.07	0.04	0.78
0.52	0.00	0.17	0.12	0.01	0.02	0.04
73.94	0.08	13.16	1.57	0.06	0.03	0.75
74.80	0.08	12.95	1.62	0.07	0.05	0.75
74.31	0.08	13.15	1.54	0.08	0.06	0.75
74.99	0.08	12.78	1.67	0.08	0.05	0.76
73.36	0.08	13.03	1.52	0.06	0.06	0.72
73.87	0.09	13.08	1.48	0.06	0.05	0.74
73.51	0.09	12.96	1.66	0.07	0.07	0.73
75.02	0.08	13.09	1.51	0.07	0.06	0.75
73.43	0.07	12.83	1.55	0.06	0.08	0.70
73.77	0.08	13.11	1.38	0.07	0.06	0.78
74.23	0.07	12.92	1.72	0.08	0.05	0.76
74.37	0.08	13.09	1.61	0.06	0.04	0.77
74.70	0.08	13.14	1.66	0.07	0.02	0.78
74.85	0.08	13.05	1.57	0.07	0.04	0.79
72.92	0.08	12.88	1.54	0.08	0.03	0.77
74.42	0.08	13.48	1.59	0.07	0.04	0.71
74.16	0.08	13.04	1.57	0.07	0.05	0.75
0.64	0.00	0.16	0.08	0.01	0.02	0.03
73.14	0.05	12.77	1.49	0.04	0.02	0.68
75.06	0.10	13.45	1.61	0.10	0.06	0.79
53.57	2.28	13.27	12.62	0.20	3.69	7.11
54.47	2.31	13.23	12.65	0.20	3.52	7.20
55.66	2.28	13.09	12.16	0.20	3.55	7.12
55.11	2.29	13.00	12.75	0.19	3.54	7.06
54.76	2.28	13.02	12.64	0.19	3.46	6.96
55.22	2.27	13.53	12.22	0.20	3.48	7.18
54.76	2.29	13.14	12.65	0.21	3.49	7.24
54.28	2.28	13.26	12.89	0.21	3.57	6.99

54.73	2.29	13.19	12.57	0.20	3.54	7.11
0.64	0.01	0.17	0.25	0.01	0.07	0.10

53.93	2.29	13.47	11.97	0.20	3.64	7.13
54.79	2.28	13.30	12.54	0.20	3.54	7.31
53.69	2.27	13.30	12.92	0.20	3.64	7.12
53.49	2.27	13.60	12.24	0.19	3.73	7.38
54.75	2.28	13.38	12.80	0.20	3.69	7.50
54.15	2.28	13.72	12.63	0.21	3.71	7.19
54.13	2.28	13.29	12.19	0.20	3.55	7.34
54.52	2.26	13.30	12.43	0.18	3.59	7.30
54.78	2.28	13.40	12.48	0.20	3.69	7.38
54.45	2.28	13.53	12.51	0.21	3.62	7.12
53.89	2.29	13.36	12.66	0.19	3.63	7.02
54.03	2.28	13.08	12.53	0.20	3.57	7.00
54.44	2.28	13.34	12.23	0.22	3.52	7.31
53.68	2.29	13.54	12.54	0.22	3.34	7.27
54.63	2.28	13.45	12.68	0.20	3.73	7.27
55.18	2.30	13.15	11.98	0.20	3.67	6.92
54.77	2.28	13.46	12.11	0.20	3.68	7.45
53.92	2.27	13.38	12.37	0.20	3.45	7.07
55.38	2.29	12.89	11.91	0.20	3.43	7.18
54.77	2.27	13.32	13.10	0.20	3.58	7.14

54.37	2.28	13.36	12.44	0.20	3.60	7.22
0.51	0.01	0.18	0.31	0.01	0.10	0.15

53.30	2.21	13.30	12.42	N/A	3.54	7.01
55.00	2.31	13.70	14.00	N/A	3.64	7.23

f ATK 508-09cm)

Recommended values for the Lipari from Kuehn et al. (2011) and

Na2O	K2O	P2O5	Total	Comment
4.03	5.23	0.02	99.22	Lipari
4.06	5.15	0.00	99.51	Lipari
3.88	5.35	0.01	99.62	Lipari
3.84	5.24	0.01	98.72	Lipari
3.87	5.17	0.00	97.74	Lipari
3.82	5.08	0.00	99.14	Lipari
3.81	5.18	0.01	97.79	Lipari
3.90	5.20	0.01	98.82	AVERAGE
0.10	0.08	0.01	0.78	Stdev
4.21	5.21	0.01	99.03	Lipari
3.98	5.20	0.01	99.52	Lipari
4.38	5.20	0.00	99.54	Lipari
4.12	5.19	0.01	99.73	Lipari
4.07	5.09	0.01	98.00	Lipari
4.10	5.21	0.00	98.68	Lipari
4.17	5.15	0.00	98.41	Lipari
3.96	5.44	0.01	99.99	Lipari
4.18	5.17	0.00	98.07	Lipari
4.17	5.11	0.00	98.52	Lipari
4.09	5.15	0.00	99.06	Lipari
4.17	5.33	0.01	99.51	Lipari
4.33	5.35	0.00	100.13	Lipari
3.98	5.17	0.00	99.61	Lipari
4.20	5.26	0.00	97.76	Lipari
4.07	5.24	0.00	99.69	Lipari
4.14	5.22	0.00	99.08	AVERAGE
0.12	0.09	0.01	0.75	Stdev
3.78	4.87	-0.01		
4.34	5.39	0.02		
3.08	1.85	0.34	98.00	BCR2g
2.66	1.79	0.36	98.40	BCR2g
3.22	1.84	0.34	99.46	BCR2g
3.08	1.75	0.32	99.08	BCR2g
3.02	1.80	0.34	98.48	BCR2g
3.16	1.81	0.34	99.41	BCR2g
3.24	1.79	0.34	99.15	BCR2g
3.13	1.84	0.32	98.77	BCR2g

3.07	1.81	0.34	98.84 AVERAGE
0.18	0.03	0.01	0.52 St dev

3.30	1.75	0.34	98.02 BCR2g
3.30	1.79	0.38	99.44 BCR2g
3.15	1.83	0.35	98.46 BCR2g
3.30	1.80	0.35	98.36 BCR2g
2.29	1.83	0.36	99.06 BCR2g
2.83	1.82	0.35	98.89 BCR2g
3.30	1.78	0.29	98.35 BCR2g
3.38	1.77	0.28	99.02 BCR2g
3.15	1.89	0.29	99.53 BCR2g
3.14	1.73	0.31	98.89 BCR2g
3.10	1.90	0.31	98.35 BCR2g
3.28	1.89	0.38	98.24 BCR2g
3.41	1.86	0.36	98.97 BCR2g
3.23	1.79	0.29	98.20 BCR2g
3.09	1.89	0.30	99.51 BCR2g
3.32	1.80	0.31	98.82 BCR2g
3.52	1.73	0.31	99.50 BCR2g
3.41	1.89	0.32	98.27 BCR2g
3.01	1.89	0.29	98.49 BCR2g
3.31	1.73	0.32	99.73 BCR2g

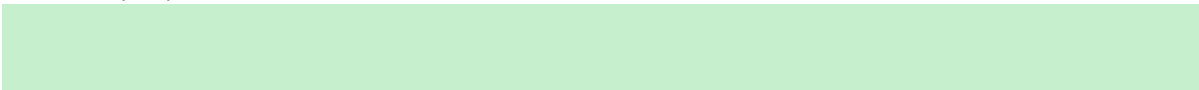
3.19	1.82	0.32	98.80 AVERAGE
0.26	0.06	0.03	0.52 St dev

3.05	1.74	0.33	
3.27	1.84	0.37	98.49


(2011) and for BCR2G from http://minerals.cr.usgs.gov/geo_chem_stand/basaltbcr2.html (accessed 12/06/13) are shown

Date

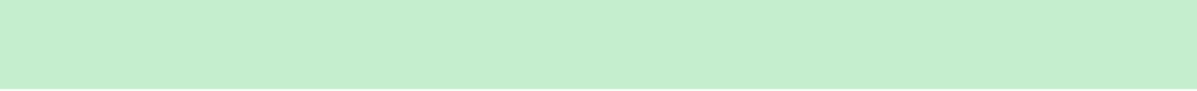
07/11/2015 09:32
07/11/2015 09:37
07/11/2015 09:43
07/11/2015 19:56
07/11/2015 20:01
07/11/2015 20:06
07/11/2015 20:12



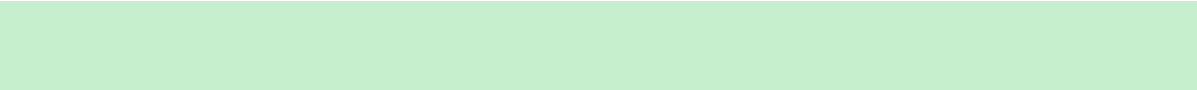
29/02/2016 11:05
29/02/2016 11:10
29/02/2016 11:15
29/02/2016 19:07
29/02/2016 19:12
29/02/2016 19:18
29/02/2016 20:11
29/02/2016 20:16
01/03/2016 03:33
01/03/2016 03:38
01/03/2016 03:44
01/03/2016 03:49
01/03/2016 03:54
01/03/2016 03:59
01/03/2016 04:05
01/03/2016 04:10



07/11/2015 09:49
07/11/2015 09:54
07/11/2015 09:59
07/11/2015 19:29
07/11/2015 19:34
07/11/2015 19:39
07/11/2015 19:45
07/11/2015 19:50



29/02/2016 10:49
29/02/2016 10:54
29/02/2016 10:59
29/02/2016 11:26
29/02/2016 11:31
29/02/2016 11:36
29/02/2016 19:28
29/02/2016 19:33
29/02/2016 19:39
29/02/2016 19:44
29/02/2016 19:50
29/02/2016 19:57
29/02/2016 20:04
01/03/2016 02:56
01/03/2016 03:02
01/03/2016 03:07
01/03/2016 03:12
01/03/2016 03:17
01/03/2016 03:23
01/03/2016 03:28



accessed 12/06/13) are shown in red.

